

## A model for turbulent mixing based on shadow-position conditioning

Stephen B. Pope

Citation: *Phys. Fluids* **25**, 110803 (2013); doi: 10.1063/1.4818981

View online: <http://dx.doi.org/10.1063/1.4818981>

View Table of Contents: <http://pof.aip.org/resource/1/PHFLE6/v25/i11>

Published by the AIP Publishing LLC.

---

### Additional information on Phys. Fluids

Journal Homepage: <http://pof.aip.org/>

Journal Information: [http://pof.aip.org/about/about\\_the\\_journal](http://pof.aip.org/about/about_the_journal)

Top downloads: [http://pof.aip.org/features/most\\_downloaded](http://pof.aip.org/features/most_downloaded)

Information for Authors: <http://pof.aip.org/authors>

### ADVERTISEMENT



**Running in Circles Looking  
for the Best Science Job?**

Search hundreds of exciting  
new jobs each month!

<http://careers.physicstoday.org/jobs>

physicstodayJOBS



## A model for turbulent mixing based on shadow-position conditioning

Stephen B. Pope<sup>a)</sup>

*Sibley School of Mechanical and Aerospace Engineering, Cornell University,  
254 Upson Hall, Ithaca, New York 14853, USA*

(Received 30 December 2012; accepted 19 March 2013; published online 26 August 2013)

In the modeling and simulation of mixing and reaction in turbulent flows using probability density function (PDF) methods, a key component is the *mixing model*, which represents the mixing effected by molecular diffusion. A new model, called the *shadow-position mixing model* (SPMM), is introduced and its performance is illustrated for two test cases. The model involves a new variable—the *shadow position*—and mixing is modeled as a relaxation of the composition to its mean conditional on the shadow position. The model is constructed to be consistent with turbulent dispersion theory, and to be local in the composition space, both to adequate approximations. The connections between the SPMM and previous mixing models are discussed. The first test case of a scalar mixing layer shows that the SPMM yields scalar statistics in broad agreement with experimental data. The second test case of a reactive scalar mixing layer with idealized non-premixed combustion shows that the SPMM correctly yields stable combustion, whereas simpler models incorrectly lead to extinction. The model satisfies all required realizability and transformation properties and correctly yields Gaussian distributions in appropriate circumstances. The SPMM is generally applicable to turbulent reactive flows using different PDF approaches in the contexts of both Reynolds-averaged Navier-Stokes modeling and large-eddy simulation. © 2013 AIP Publishing LLC. [<http://dx.doi.org/10.1063/1.4818981>]

### I. INTRODUCTION

The molecular mixing of different chemical species is of fundamental importance in numerous applications including combustion, chemical processing, and environmental flows;<sup>1</sup> and the treatment of this mixing process is a central issue in all modeling and simulation approaches to the turbulent flows in such applications. In the present work we introduce and examine a new model of molecular mixing in the context of probability density function (PDF) methods,<sup>2-4</sup> which are used extensively for turbulent reactive flows in both Reynolds-averaged Navier-Stokes (RANS) and large-eddy simulation (LES) frameworks.<sup>5-7</sup>

We take the Lagrangian viewpoint and consider modeling the evolution of the properties of a fluid particle whose position, velocity, and composition at time  $t$  are denoted by  $\mathbf{X}^*(t)$ ,  $\mathbf{U}^*(t)$ , and  $\phi^*(t)$ . In general, the composition  $\phi$  may be a set of species mass fractions and enthalpy, but we also consider a single conserved passive scalar, denoted by  $\phi$ . (In the standard notation used,  $\phi(\mathbf{x}, t)$  denotes the Eulerian composition field, and  $\phi^*(t)$  denotes a model for the composition following a fluid particle.)

To introduce the principal ideas, we consider the simplest case of high-Reynolds-number, homogeneous, isotropic turbulence. In this case, the velocity is quite accurately modeled by the Langevin equation,<sup>8,9</sup> so that  $\mathbf{X}^*$  and  $\mathbf{U}^*$  evolve by

---

<sup>a)</sup>Electronic mail: [s.b.pope@cornell.edu](mailto:s.b.pope@cornell.edu)

$$\frac{d\mathbf{X}^*}{dt} = \mathbf{U}^*, \quad (1)$$

$$d\mathbf{U}^* = -\mathbf{U}^* \frac{dt}{T_L} + \left(\frac{2\sigma^2}{T_L}\right)^{1/2} d\mathbf{W}, \quad (2)$$

where  $\sigma$  is the rms velocity,  $T_L$  is the Lagrangian integral time scale, and  $\mathbf{W}(t)$  is an isotropic Wiener process.

The simplest turbulent mixing model is the *interaction-by-exchange with the mean* (IEM) model<sup>10</sup> or, equivalently, the *linear mean-square estimation* (LMSE) model,<sup>11</sup> according to which  $\phi^*(t)$  evolves by

$$\frac{d\phi^*}{dt} = -\frac{c_\phi}{T_L}(\phi^* - \langle \phi^* | \mathbf{X}^* \rangle), \quad (3)$$

where  $c_\phi$  is a model coefficient, and  $\langle \phi^* | \mathbf{X}^* \rangle$  denotes the mean of  $\phi^*$  conditional upon  $\mathbf{X}^*$ . As is appropriate to turbulent mixing at high Reynolds number, the rate of mixing is modeled to be determined by the integral time scale, independent of the molecular diffusivity.

While the IEM model is widely used and indeed is useful, it has several deficiencies.<sup>3,12,13</sup> In the present context, the two most significant deficiencies—explained below—are that it is inconsistent with turbulent dispersion theory, and it is non-local in composition space.

According to Taylor's theory of turbulent dispersion,<sup>14</sup> at high Reynolds number the mean composition field  $\langle \phi(\mathbf{x}, t) \rangle \equiv \langle \phi^*(t) | \mathbf{X}^*(t) = \mathbf{x} \rangle$  is determined entirely by the motion of the fluid, and is unaffected by molecular diffusion. A consequence is that the scalar flux  $\langle \mathbf{U}\phi \rangle$  is unaffected by molecular mixing, and so also therefore is its rate of change.<sup>15</sup> It follows that a mixing model that is consistent with dispersion theory satisfies

$$\left\langle \mathbf{U}^* \frac{d\phi^*}{dt} | \mathbf{X}^* \right\rangle = 0, \quad (4)$$

which we refer to as the *dispersion-consistency condition*. Clearly the IEM model does not satisfy this condition, but instead yields

$$\left\langle \mathbf{U}^* \frac{d\phi^*}{dt} | \mathbf{X}^* \right\rangle = -\frac{c_\phi}{T_L} \langle \mathbf{U}^* \phi^*(t) | \mathbf{X}^* \rangle. \quad (5)$$

The *interaction by exchange with the conditional mean* (IECM) mixing model<sup>16,17</sup> was introduced to overcome this deficiency, and it has indeed proven successful for dispersion problems for which the IEM model is grossly inaccurate.<sup>18,19</sup> In the IECM model, the composition evolves by

$$\frac{d\phi^*}{dt} = -\frac{c_U}{T_L}(\phi^* - \langle \phi^* | \mathbf{U}^*, \mathbf{X}^* \rangle), \quad (6)$$

where  $c_U$  is a model coefficient, so that the relaxation is towards the mean conditioned on velocity as well as on position.

The second significant deficiency of the IEM model is that it is non-local in composition space. From the usual continuum viewpoint, molecular diffusion is an exchange of composition between neighboring fluid particles which are infinitesimally close in both position and in composition. In contrast, in IEM the exchange (between  $\phi^*$  and its mean  $\langle \phi^* | \mathbf{X}^* \rangle$ ) is non-local in composition space (although local in position). As discussed by Norris and Pope<sup>20</sup> and below in Sec. V, this deficiency can be very serious in combustion applications: it can, for example, erroneously cause extinction of a non-premixed turbulent flame at infinite Damköhler number.

The *Euclidean minimum spanning tree* (EMST) mixing model<sup>13</sup> was developed to remedy this non-localness deficiency of the IEM model, which it does. In comparative tests of mixing models applied to non-premixed turbulent flames,<sup>21</sup> the EMST model is found to be the most accurate.

However, the model has its own set of deficiencies, among which are the following:

1. It is a numerical method implemented for a set of  $N$  particles, and the convergence as  $N$  tends to infinity is uncertain.
2. It violates the linearity and independence principles applicable to a set of conserved passive scalars.<sup>22</sup>
3. It does not yield Gaussian PDFs in appropriate circumstances.
4. It is prone to “stranding” of particles in composition space (as described in Ref. 13).

The *shadow-position* mixing model (SPMM) introduced here is, to a good approximation, consistent with dispersion theory and local in composition space. It draws on some of the ideas of *multiple mapping conditioning* (MMC),<sup>23–25</sup> in particular by introducing *conditioning variables*. As described fully in Sec. II, we introduce the *shadow position*  $\mathbf{Z}^*(t)$  as an additional particle property, and then model mixing by

$$\frac{d\phi^*}{dt} = -\frac{c}{T_L}(\phi^* - \langle \phi^* | \mathbf{Z}^*, \mathbf{X}^* \rangle), \quad (7)$$

where  $c$  is a model coefficient. In addition to (approximate) dispersion-consistency and localness, favorable attributes of the shadow-position mixing model are that it satisfies linearity and independence, it yields Gaussian PDFs in appropriate circumstances, and it completely avoids “stranding.” (Like all the models mentioned above, it also satisfies the more basic requirements of preserving the mean and the boundedness of the composition distribution, and causing the variance to decrease.)

While the SPMM has connections to IEM, IECM, MMC, and EMST, we also mention that other mixing models used in PDF methods include Curl’s model,<sup>26</sup> the modified Curl model (MC),<sup>27</sup> the binomial Langevin model,<sup>28</sup> and the parameterized scalar profile (PSP) model.<sup>29–31</sup>

The outline of the remainder of the paper is as follows. The equations governing the shadow-position mixing model are presented in Sec. II, with minimal explanation. Then, in Sec. III the model is applied to the simple case of a uniform mean scalar gradient in homogeneous isotropic turbulence. This serves to clearly reveal the important properties of the shadow-position mixing model, and to provide a rational way to specify the model coefficients. In Sec. IV the SPMM is applied to the scalar mixing layer in a mildly strained flow, which allows a direct comparison with the mean obtained from dispersion theory, and a qualitative comparison with the experimental data on the scalar variance, skewness, and kurtosis obtained by Ma and Warhaft<sup>32</sup> in a slightly different scalar mixing layer. In Sec. V mixing models are applied to a turbulent non-premixed flame test case, based on that studied by Norris and Pope,<sup>20</sup> and it is shown that the SPMM correctly yields stable combustion, whereas both the IEM and IECM models incorrectly lead to extinction. Various aspects of the model and its extensions are discussed in Sec. VI; and a summary and conclusions are provided in Sec. VII.

An important issue is the accurate and efficient computational implementation of the shadow-position mixing model. We use a mesh-free, near-neighbor implementation, which is briefly described in Sec. VI D, and which will be more thoroughly described and tested in a forthcoming publication. Suffice it to say that care has been taken to ensure that all of the results presented below are numerically accurate.

In Sec. VI E we describe an extension—the velocity-shadow-position mixing model (VSPMM)—which exactly satisfies dispersion consistency, and can satisfy localness either exactly or approximately. Because of these favorable attributes, the model is of theoretical interest, but it is less amenable than SPMM to numerical implementation for statistically inhomogeneous flows.

## II. THE SHADOW-POSITION MIXING MODEL

To the general fluid particle with position  $\mathbf{X}^*(t)$  we associate a *shadow particle* with position  $\mathbf{Z}^*(t)$ . This *shadow position*  $\mathbf{Z}^*(t)$  is defined to evolve by the stochastic differential equation (SDE)

$$d\mathbf{Z}^* = \langle \mathbf{U}^* | \mathbf{X}^* \rangle dt - \frac{a}{T_L}(\mathbf{Z}^* - \mathbf{X}^*) dt + b(2\sigma^2 T_L)^{1/2} d\mathbf{W}', \quad (8)$$

where  $a$  and  $b$  are positive coefficients (whose values are considered in Sec. III), and  $\mathbf{W}'$  is an isotropic Wiener process, independent of that in the Langevin equation (Eq. (2)). The three terms on the right-hand side correspond to: movement with the local mean velocity; relaxation towards the fluid particle position; and a random walk.

The name “shadow” is deserved based on two different meanings of the word. First, the shadow particle is “an inseparable companion or follower” of the fluid particle. Second, for a given fluid particle,  $\mathbf{Z}^*$  is random with a distribution resembling a penumbral shadow behind the fluid particle. For example, for a fluid particle moving with velocity  $\langle \mathbf{U}^* | \mathbf{X}^* \rangle + \mathbf{V}$ , for a fixed value of  $\mathbf{V}$ , the distribution of  $\mathbf{Z}^*$  is an isotropic joint normal, with its center displaced by  $-\mathbf{V}T_L/a$  from the fluid particle, and with standard deviation  $\sigma T_L b/\sqrt{a}$ .

It is convenient to introduce the *shadow displacement* defined by

$$\mathbf{R}^*(t) \equiv \mathbf{Z}^*(t) - \mathbf{X}^*(t). \quad (9)$$

It follows from Eqs. (1) and (8) that this evolves by

$$d\mathbf{R}^* = -a\mathbf{R}^* \frac{dt}{T_L} - (\mathbf{U}^* - \langle \mathbf{U}^* | \mathbf{X}^* \rangle) dt + b(2\sigma^2 T_L)^{1/2} d\mathbf{W}'. \quad (10)$$

It is obvious from Eq. (9) that  $\{\mathbf{Z}^*, \mathbf{X}^*\}$  and  $\{\mathbf{R}^*, \mathbf{X}^*\}$  contain the same information, and hence conditioning on one is identical to conditioning on the other. Hence, the shadow-position mixing equation, Eq. (7), can be written as

$$\frac{d\phi^*}{dt} = -\frac{c}{T_L}(\phi^* - \langle \phi^* | \mathbf{R}^*, \mathbf{X}^* \rangle). \quad (11)$$

We take the above two equations, Eqs. (10) and (11), to be the defining equations of the shadow-position mixing model.

### III. APPLICATION TO A UNIFORM MEAN SCALAR GRADIENT

#### A. Description of the flow

We consider statistically stationary, homogeneous, isotropic turbulence, characterized by the rms velocity  $\sigma$  and the Lagrangian integral time scale  $T_L$ . There is a single, conserved, passive scalar denoted by  $\Phi(\mathbf{x}, t)$ . There is a constant and uniform mean gradient  $\partial\langle\Phi\rangle/\partial x = G$ , where  $x$  is a coordinate in the direction of the gradient. Thus, with a suitable choice of origin, the mean scalar field is given by

$$\langle\Phi\rangle = Gx. \quad (12)$$

The fluctuation in the scalar  $\phi(\mathbf{x}, t)$  is then

$$\phi \equiv \Phi - \langle\Phi\rangle = \Phi - Gx. \quad (13)$$

The specified initial condition (at  $t = 0$ ) is that there are no scalar fluctuations, i.e.,  $\phi(\mathbf{x}, 0) = 0$ .

This flow is statistically homogeneous, and it is sufficient to consider the single component of velocity in the direction of the mean scalar gradient, which we denote by  $U$ . The primary statistics of interest are the scalar variance  $\langle\phi^2\rangle$  and the scalar flux  $\langle U\phi\rangle$ , which we express in normalized form as

$$V_\phi(t) \equiv \frac{\langle\phi^2\rangle}{(G\sigma T_L)^2} \quad (14)$$

and

$$F_\phi(t) \equiv \frac{\langle U\phi\rangle}{G\sigma^2 T_L}. \quad (15)$$

This flow has been studied using Direct Numerical Simulation (DNS),<sup>33,34</sup> and there have been experiments on the similar flow in decaying grid turbulence.<sup>35</sup> The principal relevant observations

from the DNS are as follows:

1. The one-point, one-time statistics of  $U$  and  $\phi$  are joint normal.
2. For sufficiently large times the flow becomes statistically stationary.
3. In the statistically stationary state, the scalar flux correlation coefficient is

$$\rho_{U\phi} \equiv \frac{\langle U\phi \rangle}{\sigma \langle \phi^2 \rangle^{1/2}} \approx -0.55, \quad (16)$$

with no discernible Reynolds-number dependence.

Application of Taylor's theory of turbulent dispersion to this flow shows that the scalar flux is given by

$$\langle U\phi \rangle = -\hat{\Gamma}_T(t) \frac{\partial \langle \Phi \rangle}{\partial x}, \quad (17)$$

where the time-dependent turbulent diffusivity is given by<sup>8</sup>

$$\hat{\Gamma}_T(t) = \sigma^2 \int_0^t \rho_L(s) ds, \quad (18)$$

where  $\rho_L(s)$  is the two-time Lagrangian velocity autocorrelation function. In the statistically stationary state this yields

$$\Gamma_T \equiv \hat{\Gamma}_T(\infty) = \sigma^2 \int_0^\infty \rho_L(s) ds = \sigma^2 T_L, \quad (19)$$

where the last step follows from the definition of  $T_L$ .

From Eqs. (15), (17), and (19), we observe that, in the statistically stationary state, the normalized scalar flux is

$$F_\phi(\infty) \equiv \frac{\langle U\phi \rangle}{G\sigma^2 T_L} = -1. \quad (20)$$

This equation is used in two ways. First, it is used to extract the value of  $T_L$  from the DNS, based on the reported values of  $G$ ,  $\sigma$ , and  $\langle U\phi \rangle$ . Second, it provides the dispersion-consistency condition (in the statistically stationary state). Furthermore, from Eqs. (14), (16), and (20), it follows that in the statistically stationary state the normalized scalar variance is

$$V_\phi(\infty) = \rho_{U\phi}^{-2} \approx 3.3. \quad (21)$$

## B. Shadow-position model equations

For this flow, the relevant particle properties are velocity  $U^*(t)$ , shadow displacement  $R^*(t)$ , and scalar fluctuation  $\phi^*(t)$ . The position of the particle is immaterial, since the flow is statistically homogeneous. Note that  $U^*$  and  $R^*$  are the components of  $\mathbf{U}^*$  and  $\mathbf{R}^*$  in the direction of the mean scalar gradient.

The evolution equations for these quantities are

$$dU^* = -U^* \frac{dt}{T_L} + \left( \frac{2\sigma^2}{T_L} \right)^{1/2} dW, \quad (22)$$

$$dR^* = -aR^* \frac{dt}{T_L} - U^* dt + b(2\sigma^2 T_L)^{1/2} dW', \quad (23)$$

$$\frac{d\phi^*}{dt} = -GU^* - \frac{c}{T_L} (\phi^* - \langle \phi^* | R^* \rangle), \quad (24)$$

where  $W(t)$  and  $W'(t)$  are independent, scalar-valued Wiener processes. The equations for  $U^*$  and  $R^*$  are simply the scalar versions of Eqs. (2) and (10), with the mean velocity appropriately set to

zero. The equation for  $\phi^*$  is derived from Eqs. (11) and (13): the term in  $G$  arises due to the changing mean as the particle moves in  $x$ ; and, in the term in  $c$ , the conditioning is on only  $R^*$ , again because of statistical homogeneity.

The appropriate initial conditions are discussed below (in Sec. III F). For the moment, it is sufficient to stipulate that  $\{U^*(0), R^*(0), \phi^*(0)\}$  is joint normal with zero means. For then, the solution to the above equations remains Gaussian for all time. This follows from two observations. First, with  $R^*$  and  $\phi^*$  being joint normal, the conditional mean in Eq. (24) is

$$\langle \phi^* | R^* \rangle = R^* \frac{\langle R^* \phi^* \rangle}{\langle R^{*2} \rangle}. \quad (25)$$

Second, given this result, the evolution equations, Eqs. (22)–(24), form a set of linear stochastic differential equations, which are known to yield Gaussian statistics.<sup>36</sup>

### C. Statistically stationary state

Since the solution to the SDEs is Gaussian, the one-time joint PDF of the particle properties is completely determined by their means, which are zero, and by their second moments. In Appendix A, the evolution equations for the second moments are derived from Eqs. (22)–(25), and their solutions are obtained for the statistically stationary state. The principal observations (pertaining to the statistically stationary state) are as follows:

1. The dispersion-consistency condition is satisfied if the correlation coefficients satisfy the relation

$$\rho_{U\phi} = \rho_{UR}\rho_{R\phi}, \quad (26)$$

which requires  $R^*$  to be more strongly correlated with both  $U^*$  and  $\phi^*$  than the latter two quantities are with each other. (The obvious notation is that  $\rho_{U\phi}$  denotes the correlation coefficient between  $U^*$  and  $\phi^*$ , Eq. (16), etc.)

2. The satisfaction of this dispersion-consistency condition is achieved with the specification of the coefficient  $b$  as

$$b = \frac{1}{1+a}. \quad (27)$$

3. With this specification of  $b$ , and with  $a$  and  $c$  strictly positive, the normalized variances of  $R^*$  and  $\phi^*$  are

$$\frac{\langle R^{*2} \rangle}{(\sigma T_L)^2} = \frac{2+a}{a(1+a)^2} \quad (28)$$

and

$$V_\phi \equiv \frac{\langle \phi^{*2} \rangle}{(G\sigma T_L)^2} = \frac{1}{c} + \frac{2+a}{a}. \quad (29)$$

4. The correlation coefficients are

$$\rho_{UR} = -\left(\frac{a}{2+a}\right)^{1/2}, \quad (30)$$

$$\rho_{U\phi} = -\left(\frac{1}{c} + \frac{2+a}{a}\right)^{-1/2}, \quad (31)$$

$$\rho_{R\phi} = \left(\frac{a}{2+a}\right)^{-1/2} \left(\frac{1}{c} + \frac{2+a}{a}\right)^{-1/2}. \quad (32)$$

#### D. Specification of the coefficients

There are three coefficients in the shadow-position mixing model:  $a$ ,  $b$ , and  $c$ . As shown above,  $b$  is determined in terms of  $a$  (Eq. (27)) by the dispersion-consistency condition. We use Eq. (29) and the value of the normalized scalar variance  $V_\phi \approx 3.3$  observed in the DNS (Eq. (21)) to determine  $c$  in terms of  $a$  as

$$c = \frac{1}{V_\phi - 1 - 2/a}. \quad (33)$$

We observe from this equation that there is a minimum value of  $a$ ,

$$a_{\min} \equiv \frac{2}{V_\phi - 1} \approx 0.87, \quad (34)$$

such that  $c$  is positive and finite for  $a > a_{\min}$ ; and Eq. (33) can be re-expressed as

$$\frac{1}{c} = 2 \left( \frac{1}{a_{\min}} - \frac{1}{a} \right). \quad (35)$$

Similarly, there is a minimum value of  $c$ , corresponding to  $a \rightarrow \infty$ , which is  $c_{\min} = a_{\min}/2 \approx 0.43$ .

For every value of  $a \geq a_{\min}$ , the model is completely consistent with the DNS data in the statistically stationary state in that the statistics of  $U^*$  and  $\phi^*$  are joint normal, with the correct first and second moments.

In order to show the dependence of the various correlation coefficients on the model parameter  $a$ , in Fig. 1 they are plotted against  $\alpha \equiv (a - a_{\min})/a$ . As  $\alpha$  increases from 0 to 1,  $a$  increases from  $a_{\min}$  to infinity,  $|\rho_{UR}|$  increases from  $|\rho_{U\phi}|$  to unity,  $\rho_{R\phi}$  decreases from unity to  $|\rho_{U\phi}|$ , while the product of  $\rho_{UR}$  and  $\rho_{R\phi}$  remains equal to the constant value of  $\rho_{U\phi}$ .

For the limiting value  $a = a_{\min}$ ,  $c$  is infinite, and the model yields no conditional fluctuations, i.e.,  $\phi^* = \langle \phi^* | R^* \rangle$ . In this case, the model is completely local in composition space. In general, we define the *degree of non-localness*,  $\mathcal{N}$ , by

$$\mathcal{N} = \frac{\text{std}(\phi^* - \langle \phi^* | R^* \rangle)}{\text{std}(\phi^*)}, \quad (36)$$

where  $\text{std}$  denotes the standard deviation. Given that  $R^*$  and  $\phi^*$  are joint-normally distributed, this expression for  $\mathcal{N}$  is readily determined to be

$$\mathcal{N} = (1 - \rho_{R\phi}^2)^{1/2}, \quad (37)$$

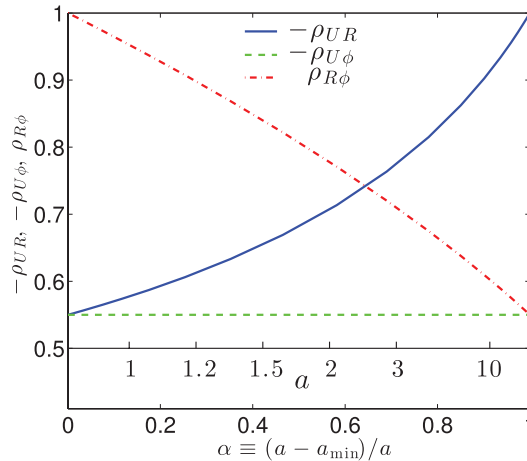


FIG. 1. Correlation coefficients in the statistically stationary state as functions of the model coefficient  $a$  expressed in terms of  $\alpha \equiv (a - a_{\min})/a$ :  $-\rho_{UR}$  (solid line);  $-\rho_{U\phi}$  (dashed line);  $\rho_{R\phi}$  (dashed-dotted line).



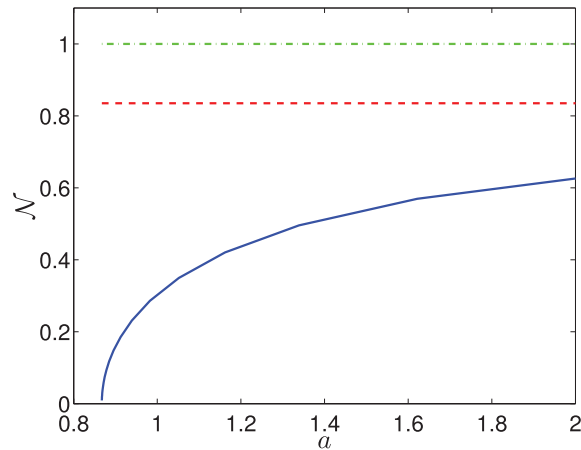


FIG. 2. Degree of non-localness  $\mathcal{N}$  (Eq. (36)) as a function of the model coefficient  $a$ : shadow-position mixing model (solid line); IECM (dashed line); IEM (dashed-dotted line).

and Eqs. (32) and (33) show that in the statistically stationary state this is simply related to the coefficient  $c$  by

$$\mathcal{N} = (cV_\phi)^{-1/2}. \quad (38)$$

Figure 2 shows  $\mathcal{N}$  as a function of the coefficient  $a$ . As may be seen, for  $a = a_{\min}$ , as previously observed, the model is completely local, with  $\mathcal{N} = 0$  and  $c = \infty$ . As  $a$  increases from  $a_{\min}$ ,  $\mathcal{N}$  increases, initially with infinite slope. Also shown are the values of  $\mathcal{N}$  for the IECM and IEM models, which are consistently defined by substituting  $\langle \phi^* | U^* \rangle$  and  $\langle \phi^* \rangle$ , respectively, for  $\langle \phi^* | R^* \rangle$  in Eq. (36). Clearly, for sufficiently small values of  $a$ , the shadow-position mixing model achieves a significantly higher degree of localness than IEM and IECM.

We now examine the transient behavior of the shadow-position mixing model for the mean scalar gradient test case. The ordinary differential equations for the second moments are integrated starting from the statistically stationary state for  $U^*$  and  $R^*$ , and with  $\phi^* = 0$ . The resulting evolution of the normalized scalar flux  $F_\phi$  is shown in Fig. 3 for different values of  $a$ . By construction of the model, specifically the satisfaction of the dispersion-consistency condition in the stationary state,

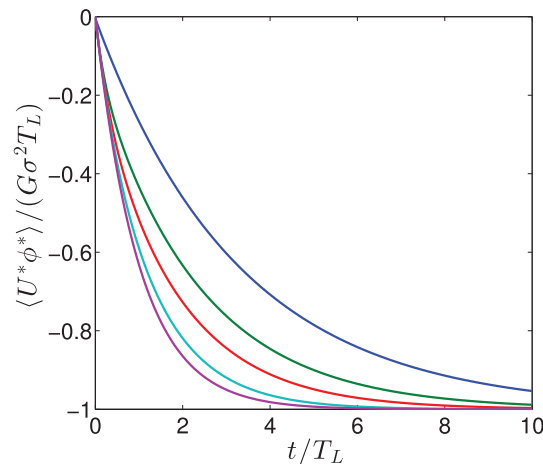


FIG. 3. Normalized scalar flux as a function of normalized time for different values of the coefficient  $a$  in the shadow-position mixing model. From top to bottom, the values of  $a$  are 0.87, 1.0, 1.2, and 2.0, and  $\infty$ . With  $a = \infty$  the result is the same as that given by dispersion theory and by the IECM model.

the scalar flux  $F_\phi$  tends to  $-1$  at large time for all values of  $a$ . For  $a = \infty$  the model is consistent with dispersion theory for all time, but as  $a$  decreases discrepancies during the transient emerge.

The specification of  $a$  therefore involves a compromise: as  $a$  increases from  $a_{\min}$ , the model becomes less local, but more consistent with dispersion theory. As the results presented below in Secs. IV and V show, a reasonable and simple specification of the coefficients is  $a = 1$ , which leads to  $b = 1/2$  and  $c = 3.27$ .

It should also be remembered that the dispersion-consistency condition applies only at large Reynolds number. At moderate Reynolds number, DNS<sup>33</sup> reveals that there is a significant correlation between velocity and molecular mixing.

### E. Reduction to other models

It is interesting to observe that, as now explained, with different limiting values of the coefficients, the shadow-position mixing model reduces to the IEM model, to the IECM model, or to generalized MMC.<sup>24</sup>

As mentioned above, in the limiting case  $a = a_{\min}$ ,  $b = 1/(1 + a)$ ,  $c \rightarrow \infty$ , there are no conditional fluctuations so that (in the general case) we have

$$\phi^*(t) = \langle \phi^*(t) | \mathbf{X}^*(t), \mathbf{R}^*(t) \rangle. \quad (39)$$

This can be viewed as a variant of deterministic generalized MMC,<sup>24,25</sup> with  $\mathbf{R}^*$  being the conditioning variable. However, SPMM differs from MMC (as originally proposed<sup>23</sup>) in that conditioning is not on all of the variables ( $\mathbf{U}^*$ ,  $\mathbf{R}^*$ ). Subsequent to the original MMC paper,<sup>23</sup> Klimenko<sup>24</sup> defined the less restrictive ‘‘generalized’’ MMC in which the conditioning variables (here  $\mathbf{R}^*$ ) are allowed to be a subset of the reference variables (here  $\mathbf{U}^*$  and  $\mathbf{R}^*$ ). For  $a \geq a_{\min}$ , the SPMM is a form of the stochastic generalized MMC model, termed MMC-IEM.<sup>24</sup> (It should be noted that generalized MMC is a broad definition, which includes IECM, which pre-dates MMC.)

The velocity-shadow-position mixing model described below (in Sec. VI E) is an MMC model in the original sense.

The IECM model is obtained by taking the limit  $a \rightarrow \infty$ ,  $b = 1/(1 + a) = 0$ , and  $c = c_{\min} = c_U$ . In this limit,  $R^*$  and  $U^*$  become perfectly correlated, so that conditioning on  $R^*$  is identical to conditioning on  $U^*$ , and the shadow-position mixing equation degenerates to the IECM equation (Eq. (6)).

The IEM model is obtained by taking  $a \rightarrow \infty$ ,  $b = \gamma\sqrt{a} \rightarrow \infty$ , and  $c = c_\phi$  for any positive value of  $\gamma$ . In this limit,  $R^*$  becomes independent of  $U^*$  and  $\phi^*$ , so that conditioning on  $R^*$  has no effect, i.e.,  $\langle \phi^* | R^* \rangle = \langle \phi^* \rangle$ , so that the shadow-position mixing equation (Eq. (7)) degenerates to the IEM equation (Eq. (3)).

### F. Initial and boundary conditions

For the case considered of passive scalar mixing in statistically stationary, homogeneous, isotropic turbulence, the only possible consistent initial condition for  $R^*$  is that it is in the statistically stationary state. Any other condition would violate the independence principle.<sup>22</sup> This is most simply seen by considering two different scalars initialized in the same way, but at times  $t = t_1 = 0$  and  $t = t_2 > 0$ . Clearly, the statistics of both scalars evolve in the same way, just with a shift in time. With the shadow-position mixing model, this requires that the distribution of  $\{U^*, R^*\}$  be the same at times  $t_1$  and  $t_2$ , and this is achieved only if  $R^*(t_1)$  is specified in the statistically stationary state.

Another way of viewing this is that, in this example,  $t = 0$  is a special time, i.e., the time at which the first scalar is initialized. If a non-stationary specification is made for  $R^*(0)$ , then the statistics of the second scalar incorrectly depend on its initialization time  $t_2$ . That is, the second scalar is incorrectly affected by the first, in violation of the independence principle. More generally, to adhere to the independence principle, initial and boundary conditions on  $R^*$  must be independent of the compositions.

For more general flows than considered here, boundary conditions are required on the vector  $\mathbf{R}^*$ , or, equivalently, on  $\mathbf{Z}^*$ . Appropriate boundary conditions are as follows:

1. For a non-turbulent inflow:  $\mathbf{R}^* = 0$ .
2. For a turbulent inflow:  $\mathbf{R}^*$  is Gaussian, with zero mean, covariance  $\langle R_i^* R_j^* \rangle = \langle R^{*2} \rangle \delta_{ij}$ , and with correlation coefficient between  $R_i^*$  and  $U_j^*$  of  $\rho_{UR} \delta_{ij}$ , where  $\langle R^{*2} \rangle$  and  $\rho_{UR}$  are given by Eqs. (28) and (30).
3. For a solid wall: reflective boundary conditions are applied to  $\mathbf{Z}^*$ , so that the shadow position remains within the flow.

### G. Performance of the IEM and IECM models

For this flow, the IECM model (Eq. (6)) satisfies all the conditions considered above. Regardless of the value of the coefficient  $c_U$  in Eq. (6),  $U^*$  and  $\phi^*$  are joint normal, and the scalar flux is consistent with dispersion theory at all time. It follows simply from the second-moment equations that the observed scalar variance in the statistically stationary state is obtained provided that the coefficient is specified as

$$c_U = \frac{1}{V_\phi - 1} \approx 0.43. \quad (40)$$

For the IEM model, the second-moment equations show that, in the statistically stationary state, the observed scalar variance is obtained with the specification

$$c_\phi = \frac{1}{2} \left[ \left( 1 + \frac{4}{V_\phi} \right)^{1/2} - 1 \right] \approx 0.24. \quad (41)$$

However, instead of being equal to  $-1$ , the normalized scalar flux is

$$F_\phi(\infty) \equiv \frac{\langle U\phi \rangle}{G\sigma^2 T_L} = -\frac{1}{1 + c_\phi} \approx -0.80, \quad (42)$$

i.e., 20% in error.

## IV. APPLICATION TO THE SCALAR MIXING LAYER

### A. Description of the flow

The scalar mixing layer provides a simple test case to study the transport and mixing predicted by the shadow-position mixing model for a flow with a statistically inhomogeneous scalar field. This flow yields a temporally evolving, statistically one-dimensional scalar field, and we denote by  $X^*$ ,  $U^*$ , and  $R^*$  the components of  $\mathbf{X}^*$ ,  $\mathbf{U}^*$ , and  $\mathbf{R}^*$ , respectively, in the inhomogeneous  $x$  direction. As in Sec. III, we consider a conserved passive scalar in statistically stationary, homogeneous, isotropic turbulence, and the same evolution equations apply to  $U^*$  and  $R^*$ , i.e., Eqs. (22) and (23).

In the present case,  $\phi^*(t)$  denotes the scalar (not its fluctuation), which evolves by (the one-component version of) Eq. (11) from the initial condition  $\phi^*(0) = H(X^*(0))$ , where  $H(x)$  is the Heaviside function.

In order to make the flow attain a statistically stationary state, the position equation is modified to

$$\frac{dX^*}{dt} = U^* - SX^*, \quad (43)$$

where  $S$  is an imposed mean strain rate, which we take to have the relatively small value  $S = 0.1/T_L$ . Note that the model equations do not take into account the effect of straining on the turbulence.

Ma and Warhaft<sup>32</sup> have studied experimentally the scalar mixing layer in grid turbulence, and there have been DNS of the same flow.<sup>37</sup> The differences compared to the test case considered here are that the turbulence is decaying, and there is no mean straining. Nevertheless, useful comparisons can be made between the measured and calculated statistics.

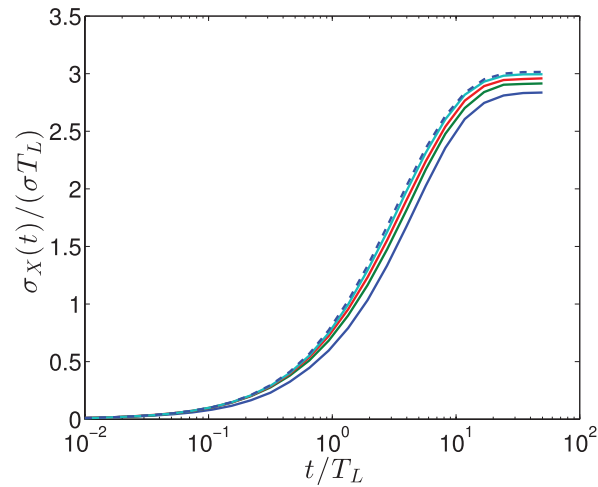


FIG. 4. Normalized width of the scalar mixing layer as a function of time. Dashed line: dispersion theory, IECM, and SPMM with  $a = \infty$ . Solid lines: SPMM with (from bottom to top)  $a = 0.87, 1.0, 1.2,$  and  $2.0$ .

## B. The mean scalar profile

The profile  $\langle \phi(x, t) \rangle$  of the mean scalar can be determined from turbulent dispersion theory, and this is done in Appendix B. The profile is an error function (Eq. (B1)) of characteristic width  $\sigma_X(t)$  given by Eq. (B10).

Numerical simulations were performed first with the IECM model, and with no mixing model (i.e.,  $d\phi^*/dt = 0$ ), both of which are consistent with dispersion theory. These calculations produce error function profiles of the correct width, which serves to verify the consistency between the simulations and the theory.

Simulations using the shadow-position mixing model for a range of values of the parameter  $a$  produce mean profiles which deviate from the error function by less than  $\frac{1}{2}\%$ . The calculated widths  $\sigma_X(t)$  are compared to the dispersion result in Fig. 4. As may be seen, the width of the scalar mixing layer increases from zero and eventually attains a constant value. The dashed line is the dispersion result, which is also given by the IECM model, and the SPMM with  $a$  infinite. As may be seen, the errors in the SPMM for finite values of  $a$  decrease as  $a$  increases. For the four values of  $a$  (0.87, 1.0, 1.2, and 2.0) the errors in the width in the statistically stationary state are 6%, 4%, 2%, and 1%, respectively.

## C. Second and higher moments

Figure 5 shows the statistically stationary profile of the rms scalar fluctuation. The coordinate  $x$  is normalized by the half-width  $L_{1/2}$  (defined such that  $\langle \phi(\pm L_{1/2}) \rangle = \frac{1}{2} \mp \frac{1}{4}$ ) to facilitate comparison with the experimental results presented by Ma and Warhaft.<sup>32</sup> It is found that the peak of the rms of  $\phi^*$  increases with  $ST_L$ , and the value used here ( $ST_L = 0.1$ ) is chosen to match approximately the experimental value. (Note that the statistics shown in Figs. 5–10 are conditioned on  $X^* = x$ , but this is not shown explicitly in the notation. Also, since the comparison between the two slightly different flows is qualitative, the experimental data are not reproduced here, but instead the reader is referred to the figures in Ma and Warhaft.<sup>32</sup>)

Figure 6 shows the profile of the (negative of the) scalar flux correlation coefficient,  $-\rho_{U\phi}$ . The shape of this profile and the peak value agree well with the experimental data.<sup>32</sup> Both for the rms and the scalar flux correlation coefficient, there is little dependence on the value of the model coefficient  $a$  over the range investigated, except for the smallest value,  $a = 0.87$ , at the edge of the layer.

Figures 7 and 8 show profiles of the skewness  $S_\phi$  and kurtosis  $\mathcal{K}_\phi$  of  $\phi^*$ . Here, there is a strong dependence on the model coefficient  $a$ . In the center of the layer, there is a linear variation of  $S_\phi$ , and the kurtosis is significantly below the Gaussian value of 3—in agreement with the

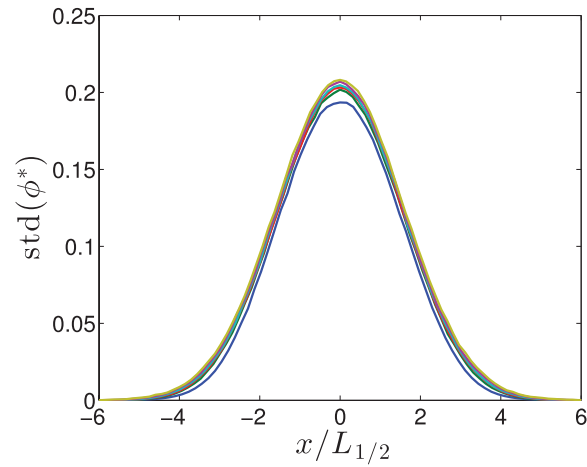


FIG. 5. Profiles of the rms of the scalar  $\phi^*$  in the scalar mixing layer in the statistically stationary state according to the SPMM for values of the coefficient  $a = 0.87, 0.91, 0.95, 1.0, 1.2,$  and  $2.0$ . The lower line is for  $a = 0.87$ .

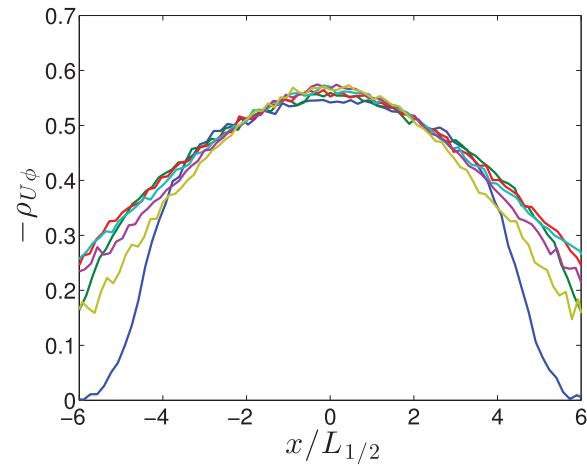


FIG. 6. Profiles of the negative of the scalar flux correlation coefficient in the scalar mixing layer in the statistically stationary state according to the SPMM for values of the coefficient  $a = 0.87, 0.91, 0.95, 1.0, 1.2,$  and  $2.0$ . The lower line is for  $a = 0.87$ .

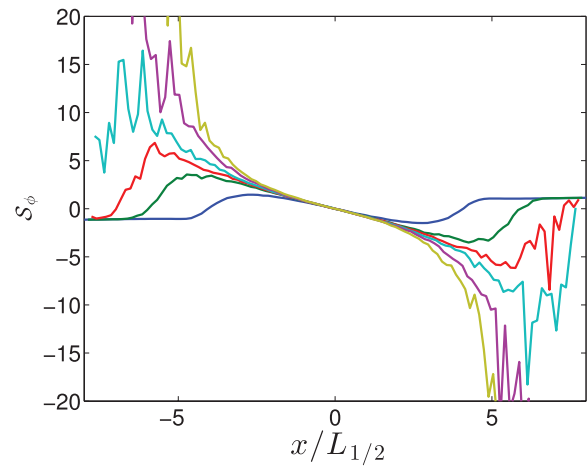


FIG. 7. Profiles of the skewness of  $\phi^*$  in the scalar mixing layer in the statistically stationary state according to the SPMM for values of the coefficient  $a = 0.87, 0.91, 0.95, 1.0, 1.2,$  and  $2.0$ . At the edges, the skewness increases in magnitude with increasing  $a$ .

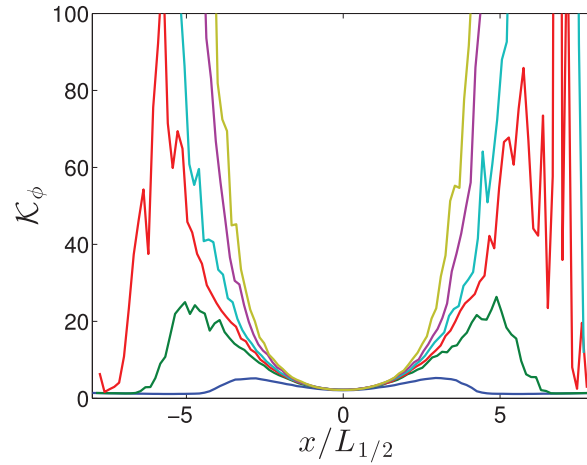


FIG. 8. Profiles of the kurtosis of  $\phi^*$  in the scalar mixing layer in the statistically stationary state according to the SPMM for values of the coefficient  $a = 0.87, 0.91, 0.95, 1.0, 1.2,$  and  $2.0$ . The kurtosis increases with increasing  $a$ .

experimental data.<sup>32</sup> At the edges of the layer, as is evident from the figures, there is considerable statistical uncertainty, even though the statistics are averaged over 40 simulations, each made with  $10^5$  particles. Nevertheless, it is clear that, at the edges, these higher moments increase strongly with  $a$ . For  $a$  greater than unity, it appears that the skewness and kurtosis tend to infinity at the edge, whereas for  $a \leq 1$  they tend to zero. For  $a = 0.91$  the peak values of the skewness and kurtosis are about 3 and 20, respectively—similar to the peak values observed by Ma and Warhaft.<sup>32</sup>

Figure 9 shows the Gaussian estimate for the fluctuation in  $\phi^*$  about its mean conditional on  $R^*$

$$\text{std}(\phi^* - \langle \phi^* | R^* \rangle)_G \equiv \text{std}(\phi^*)(1 - \rho_{R\phi}^2)^{1/2} \approx \text{std}(\phi^* - \langle \phi^* | R^* \rangle). \quad (44)$$

As expected, decreasing  $a$  towards  $a_{\min}$  causes these conditional fluctuations to decrease; for  $a = 0.87$ , they are everywhere less than 0.04.

Figure 10 shows the corresponding Gaussian estimate for the degree of non-localness

$$\mathcal{N}_G \equiv \frac{\text{std}(\phi^* - \langle \phi^* | R^* \rangle)_G}{\text{std}(\phi^*)} = (1 - \rho_{R\phi}^2)^{1/2} \approx \mathcal{N}. \quad (45)$$

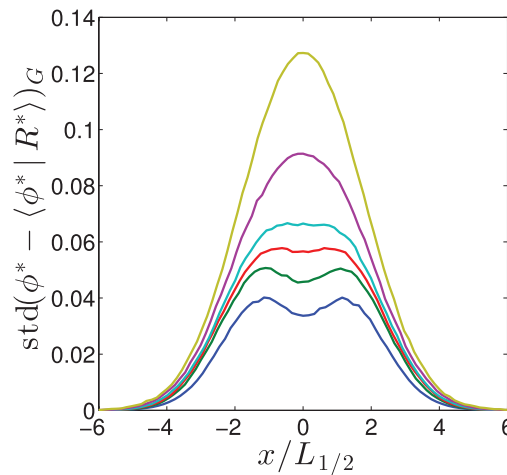


FIG. 9. Profiles of the rms of the conditional fluctuation  $\phi^* - \langle \phi^* | R^* \rangle$  (estimated by Eq. (44)) in the scalar mixing layer in the statistically stationary state according to the SPMM for values of the coefficient  $a = 0.87, 0.91, 0.95, 1.0, 1.2,$  and  $2.0$ . The rms increases with increasing  $a$ .

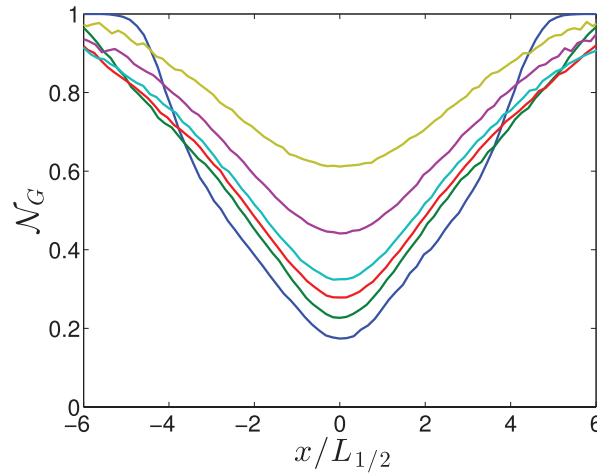


FIG. 10. Profiles of the degree of non-localness (estimated by Eq. (45)) in the scalar mixing layer in the statistically stationary state according to the SPMM for values of the coefficient  $a = 0.87, 0.91, 0.95, 1.0, 1.2,$  and  $2.0$ . In the center of the layer,  $\mathcal{N}_G$  increases with increasing  $a$ .

In the center of the layer, where the Gaussian estimate can be expected to be accurate, the values of  $\mathcal{N}_G$  are somewhat larger than the values of  $\mathcal{N}$  observed in the mean-scalar-gradient case with the same values of  $a$  (see Fig. 2). Also, the values of  $\mathcal{N}_G$  tend to unity at the edge of the layer, as the correlation coefficient  $\rho_{R\phi}$  tends to zero.

#### D. Performance of the IEM and IECM models

Calculations were also performed with the IEM and IECM models, using the values of the coefficients given by Eqs. (40) and (41). The principal observations are as follows:

1. For IECM the width  $\sigma_X(t)$  is consistent with dispersion theory at all times; whereas with IEM, in the statistically stationary state, the width is low by 9%.
2. For both models the departures from the error function profile are less than 0.2%.
3. For both models the peak scalar rms is approximately 0.21—the same as with the SPMM.
4. For both models the skewness and kurtosis tend to infinity at the edge of the layer—in qualitative disagreement with the experimental data.
5. The minimum value of the kurtosis is 1.8 for IEM and 2.1 for IECM (compared to 2.2 for SPMM).

### V. APPLICATION TO NON-PREMIXED COMBUSTION

#### A. Description of the flow

In order to test the shadow-position mixing model's ability to represent non-premixed turbulent combustion at high Damköhler number, we consider a model problem which is a combination of the scalar mixing layer considered in Sec. IV and the simple but challenging combustion model used by Norris and Pope.<sup>20</sup> We refer to this as the reactive scalar mixing layer. The flow is again constant-property, statistically stationary, homogeneous, isotropic turbulence, characterized by  $\sigma$  and  $T_L$ , with a small imposed mean strain rate  $S = 0.1/T_L$ .

In this case the fluid composition is described by two passive scalars, which we denote alternatively as  $\{\phi_1, \phi_2\} = \{\xi, Y\}$ :  $\xi$  is the mixture fraction and  $Y$  is the product mass fraction. The mixture fraction  $\xi(\mathbf{x}, t)$  is a conserved passive scalar, identical to  $\phi$  considered in Sec. IV, for which the boundary conditions are  $\xi = 0$  for  $x \rightarrow -\infty$  and  $\xi = 1$  for  $x \rightarrow \infty$ .

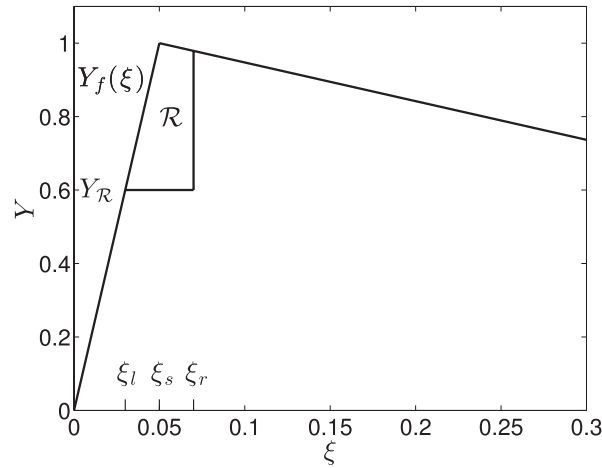


FIG. 11. Sketch of (part of) the  $\xi$ - $Y$  composition space showing the fully burnt line  $Y_f(\xi)$  and the reactive region  $\mathcal{R}$ .

Figure 11 is a sketch of part of the  $\xi$ - $Y$  composition space (which extends to  $\xi = 1$ ). The product mass fraction  $Y$  is bounded below by zero, corresponding to pure reactants, and bounded above by

$$Y_f(\xi) \equiv \min\left(\frac{\xi}{\xi_s}, \frac{1-\xi}{1-\xi_s}\right), \quad (46)$$

corresponding to fully burnt mixture, where  $\xi_s$  is the stoichiometric mixture fraction, specified to be  $\xi_s = 0.05$ .

The simple reaction model is that the reaction rate (i.e., the production rate of  $Y$ ) is infinite within the quadrilateral “reactive region”  $\mathcal{R}$  shown in Fig. 11, and it is zero elsewhere. This reactive region is defined by

$$\mathcal{R} \equiv \{(\xi, Y) \mid \xi_l < \xi \leq \xi_r, Y_{\mathcal{R}} \leq Y < Y_f(\xi)\}, \quad (47)$$

where  $\xi_l = 0.03$  and  $\xi_r = 0.07$  are the specified lean and rich limits of the reactive region, and  $Y_{\mathcal{R}}$  is taken to be 0.6. The values of the four parameters ( $\xi_s$ ,  $\xi_l$ ,  $\xi_r$ , and  $Y_{\mathcal{R}}$ ) are chosen by Norris and Pope<sup>20</sup> to be representative of methane/air and hydrogen/air combustion.

In the computations, this reaction model is simple to implement. Both particle compositions are treated as conserved passive scalars, except that, if, due to mixing,  $\{\xi^*(t), Y^*(t)\}$  moves into the reactive region, then the product mass fraction immediately jumps to the fully burnt line, i.e.,  $Y^*(t)$  is reset to  $Y^*(t) = Y_f(\xi^*(t))$ .

The initial conditions are that:  $X^*(0)$  is uniformly distributed;  $U^*(0)$  and  $R^*(0)$  are in the statistically stationary state;  $\xi^*(0)$  is set deterministically (i.e., with no fluctuations) with its mean being the error function profile, Eq. (B1), with the steady-state width  $\sigma_X(\infty)$  given by Eq. (B11); and  $Y^*(0)$  is set to its fully burnt value  $Y_f(\xi^*(0))$ .

The “correct” solution for this test case is that  $Y^*(t)$  remains on the fully burnt line for all time. Because of the infinite reaction rate, chemical reaction is confined to an infinitesimal neighborhood of  $(\xi, Y) = (\xi_s, 1)$ , and elsewhere there is inert mixing between the fully burnt stoichiometric composition  $(\xi_s, 1)$  and the two stream compositions  $(0, 0)$  and  $(1, 0)$ . This is the Burke-Schumann limit<sup>38,39</sup> in which, in physical space, reaction is confined to the stoichiometric surface  $\mathcal{S}(t) \equiv \{\mathbf{x} \mid \xi(\mathbf{x}, t) = \xi_s\}$ .

## B. Performance of the IEM and IECM models

It is instructive first to examine the performance of the IEM and IECM mixing models applied to this reactive mixing layer. For calculations using the IECM model, Fig. 12 shows scatter plots of  $(\xi^*(t), Y^*(t))$  at successive times. Recall that the correct behavior for this test case is that the composition  $(\xi^*, Y^*)$  remains on the fully burnt line. At the earliest time shown ( $t/T_L = 2$ ), the



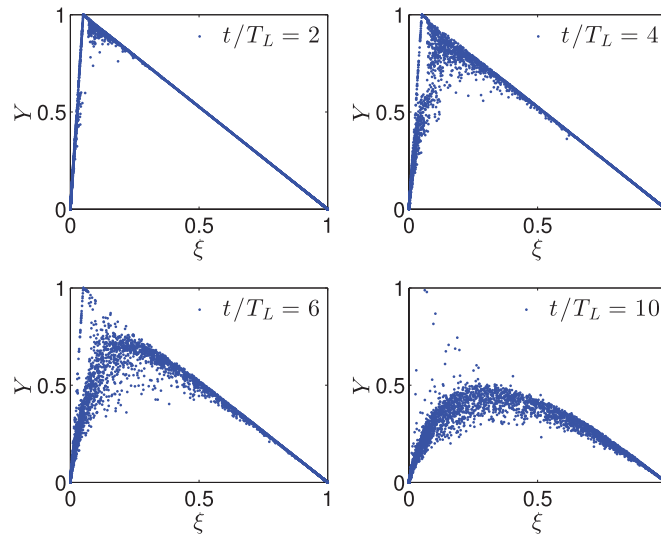


FIG. 12. Scatter plots at successive times of product mass fraction against mixture fraction in the reactive scalar mixing layer according to the IECM mixing model.

particles are predominately along the fully burnt line, and inevitably (for all times) the reactive region  $\mathcal{R}$  is void of particles. But there are some particles below the fully burnt line, most noticeably immediately to the right of  $\mathcal{R}$ . This trend of particles departing from the fully burnt line continues to the last time shown ( $t/T_L = 10$ ), when nearly all of the particles have values of  $Y^*$  less than 0.5. Subsequent complete extinction with  $Y^* \rightarrow 0$  is inevitable.

A quantification of the departures from the correct solution is provided by the conditional mean  $\langle Y | \xi \rangle \equiv \langle Y^* | \xi^* = \xi \rangle$  (which is based on all of the particles, i.e., for all  $X^*$ ). This is shown for successive times in Fig. 13. The initial condition of course shows the correct behavior  $\langle Y | \xi \rangle = Y_f(\xi)$ . However, at the next time shown ( $t/T_L = 2.2$ ), departures are evident immediately to the right of  $\mathcal{R}$ . By the final time ( $t = T_L = 50$ ) there is essentially complete extinction.

The performance of the IEM model is qualitatively the same, and quantitatively similar.

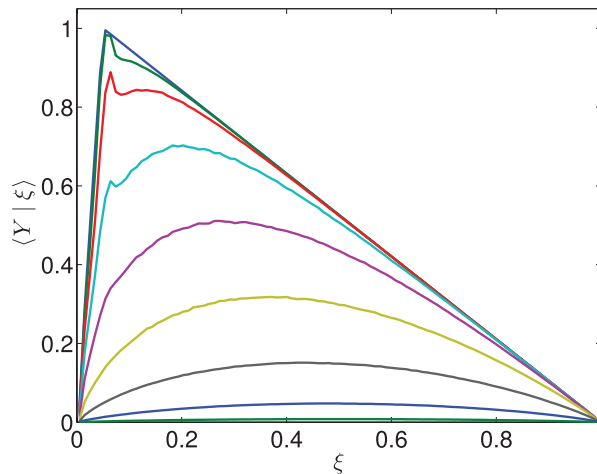


FIG. 13. The conditional mean of the product mass fraction calculated by the IECM mixing model at times (from top to bottom)  $t = 0, 2.2, 3.5, 5.4, 8.5, 13.2, 20.6, 32.1$ , and 50.

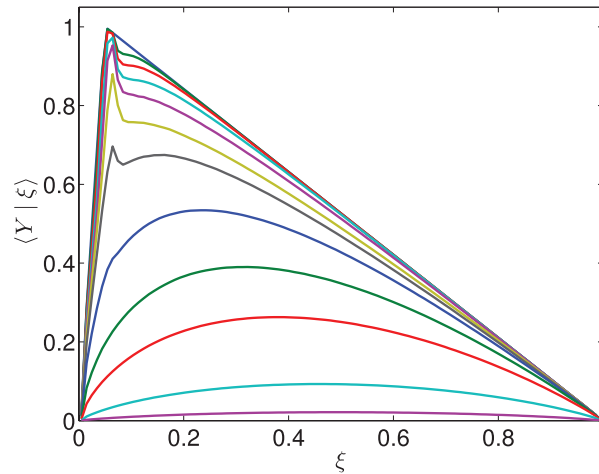


FIG. 14. The conditional mean of the product mass fraction calculated by the SPMM for  $a = 1.2$  at times (from top to bottom)  $t = 0, 3.1, 4.4, 6.2, 8.8, 12.4, 14.8, 17.6, 21.0, 24.9, 35.3,$  and  $50$ .

### C. The performance of the shadow-position mixing model

The predictions of the shadow-position mixing model for this test case depend qualitatively on the value of the model coefficient  $a$ . Figure 14 shows the temporal evolution of the conditional mean  $\langle Y | \xi \rangle$  for the case  $a = 1.2$ . As may be seen, the behavior is similar to that of the IECM model, and it shows complete extinction at large time, which is the wrong behavior. However, with the slightly smaller value  $a = 1.15$ , the behavior, shown in Fig. 15, is completely different. There is stable burning for all time, with some relatively small departures from the fully burnt line.

Figure 16 shows the temporal evolution of  $\langle Y | \xi \rangle$  for a particular value of  $\xi$ , namely  $\xi = \xi_{r+} \equiv 0.084$ , which is just to the right of the reactive region  $\mathcal{R}$ . For  $a \leq 1.15$ , stable burning is observed, with the steady-state value of  $\langle Y | \xi_{r+} \rangle$  decreasing with increasing  $a$ . On the other hand, for  $a \geq 1.2$ , extinction occurs more rapidly as  $a$  increases.

To further quantify the departures from the fully burnt line, Fig. 17 shows the “product deficit” at  $\xi_{r+}$ , defined as  $Y_f(\xi_{r+}) - \langle Y | \xi_{r+} \rangle$ . For the cases with extinction ( $a \geq 1.2$ ), this approaches  $Y_f(\xi_{r+}) \approx 0.96$  at large times; whereas for the cases with stable burning ( $a \leq 1.15$ ), the steady-state

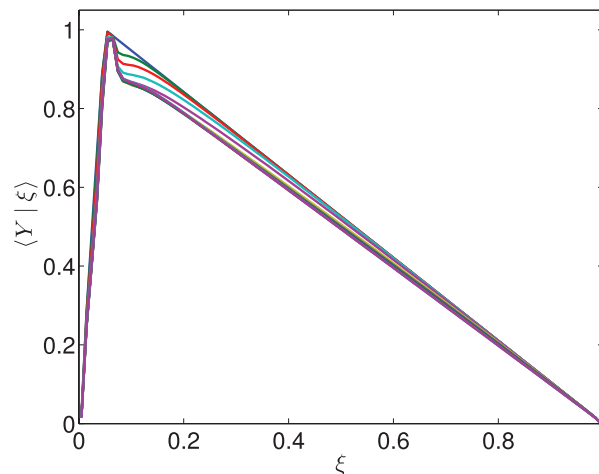


FIG. 15. The conditional mean of the product mass fraction calculated by the SPMM for  $a = 1.15$  at times (from top to bottom)  $t = 0, 3.1, 4.4, 6.2, 8.8, 12.4, 14.8, 17.6, 21.0, 24.9, 35.3,$  and  $50$ .

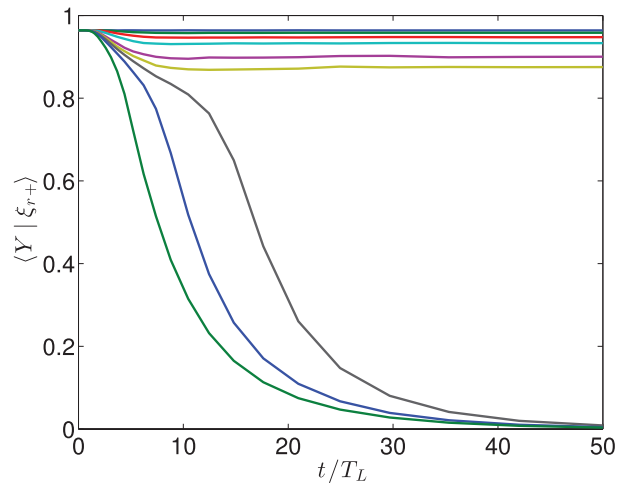


FIG. 16. The temporal evolution of the conditional mean product mass fraction for  $\xi = \xi_{r+} = 0.084$  calculated by the SPMM for (from top to bottom)  $a = 0.87, 0.91, 0.95, 1.0, 1.1, 1.15, 1.2, 1.3,$  and  $2.0$ .

value decreases towards zero (the “correct” value) as  $a$  decreases towards  $a_{\min}$ . For  $a = 0.87, 0.91,$  and  $1.15$ , the product deficit is less than  $10^{-4}, 0.006,$  and  $0.1$ , respectively.

The decreasing product deficit as  $a$  decreases towards  $a_{\min}$  is a result of the increasing localness of the shadow-position mixing model, as evidenced by the decrease in the conditional fluctuations shown in Fig. 9.

In general, there is a critical value of  $a$ ,  $a_{\text{crit}}$ , above which the model predicts extinction, and below which it predicts stable burning. For this test case, the results presented above show that  $a_{\text{crit}}$  lies between  $1.15$  and  $1.2$ . The value of  $a_{\text{crit}}$  can be expected to depend *inter alia* on the definition of the reactive region  $\mathcal{R}$ , in particular on its width in mixture fraction space  $\Delta\xi_{\mathcal{R}} \equiv \xi_r - \xi_l$ . For a smaller value of  $\Delta\xi_{\mathcal{R}}$ , it can be expected that more localness is needed for stable burning, implying a smaller value of  $a_{\text{crit}}$ . Confirming these expectations, Fig. 18 shows results for a modified test case in which  $\Delta\xi_{\mathcal{R}}$  is halved through the modified specifications  $\xi_l = 0.04$  and  $\xi_r = 0.06$ . As may be seen, for this case  $a_{\text{crit}}$  is slightly reduced to between  $1.0$  and  $1.1$ , and for a given value of  $a < a_{\text{crit}}$  the product deficit is larger. We note that the decrease in  $a_{\text{crit}}$  is not great, and that  $\Delta\xi_{\mathcal{R}} = 0.02$  is a small value compared to those in typical combustion applications. It is expected, therefore, that

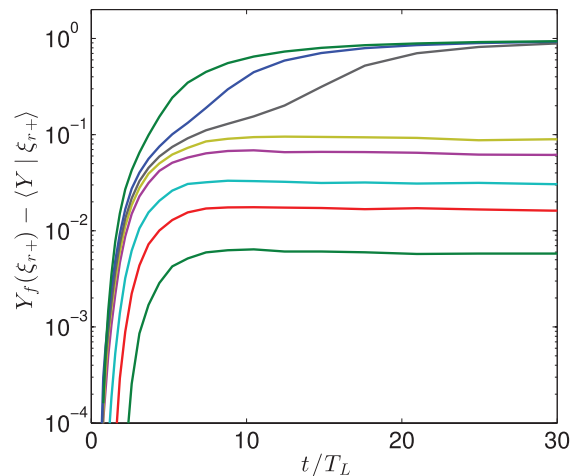


FIG. 17. The temporal evolution of the conditional product deficit for  $\xi = \xi_{r+} = 0.084$  calculated by the SPMM for (from bottom to top)  $a = 0.91, 0.95, 1.0, 1.1, 1.15, 1.2, 1.3,$  and  $2.0$ .

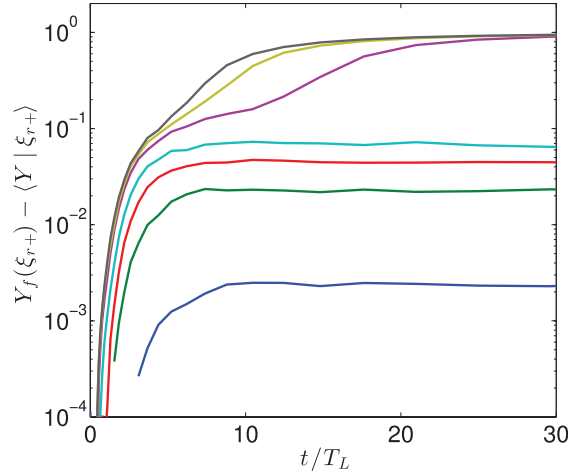


FIG. 18. For the case with  $\xi_l = 0.04$  and  $\xi_r = 0.06$ , the temporal evolution of the conditional product deficit for  $\xi = \xi_{r+} = 0.084$  calculated by the SPMM for (from bottom to top)  $a = 0.87, 0.91, 0.95, 1.0, 1.1, 1.15$ , and  $1.2$ .

the shadow-position mixing model with  $a \approx 1$  is sufficiently local to yield, correctly, stable burning when applied to turbulent non-premixed combustion at high Damköhler number.

While using  $a = a_{\min}$  achieves complete localness, it is not the best specification. This is because, with  $a = a_{\min}$ , there are no conditional fluctuations, so that, in a statistically  $D$ -dimensional flow ( $0 \leq D \leq 3$ ), the composition  $\phi^*$  is (locally) confined to a  $D$ -dimensional manifold. In contrast, it is well known that, even in statistically one-dimensional flows, the compositions occurring in combustion can lie on higher-dimensional manifolds (e.g.,  $D \geq 5$ ).<sup>7</sup> Thus, the best specification of  $a$  is between  $a_{\min}$  and  $a_{\text{crit}}$ , so that conditional fluctuations are allowed. (It is also the case that the numerical implementation of SPMM becomes increasingly demanding as  $a$  decreases towards  $a_{\min}$ .)

## VI. DISCUSSION

### A. Application to general flows

The flows considered above are extremely simple, namely, constant-property, high-Reynolds-number, homogeneous, isotropic turbulence. Nevertheless, the shadow-position model equations for  $\mathbf{R}^*$  and  $\phi^*$  (Eqs. (10) and (11)) are quite general, and are directly applicable to variable-property, inhomogeneous flows such as turbulent flames. The required initial and boundary conditions for general flows are described in Sec. III F.

We have characterized the turbulence by  $\sigma$  and  $T_L$ , which are the natural parameters for isotropic turbulence. For inhomogeneous flows, it is more normal to characterize the turbulence by its kinetic energy  $k(\mathbf{x}, t)$  and the mean dissipation rate  $\varepsilon(\mathbf{x}, t)$ ; or, in the velocity-frequency-composition PDF method, by the mean turbulence frequency,  $\Omega(\mathbf{x}, t)$ , which is analogous to  $\varepsilon/k$ . The relations between these variables are

$$\sigma^2 = \frac{2}{3}k \quad \text{and} \quad T_L = C_T \frac{k}{\varepsilon}, \quad (48)$$

where, according to the Langevin model, the constant  $C_T$  relating the Lagrangian time scale to  $k/\varepsilon$  is

$$C_T = \left( \frac{1}{2} + \frac{3}{4}C_0 \right)^{-1}, \quad (49)$$

and  $C_0$  is either taken to be a constant (e.g.,  $C_0 = 2.1$ ) or a function of the Reynolds number.<sup>9</sup> The shadow-position model equations (Eqs. (10) and (11)) re-expressed in terms of  $k$  and  $\varepsilon$  are

$$d\mathbf{R}^* = -\hat{a} \frac{\varepsilon}{k} \mathbf{R}^* dt - (\mathbf{U}^* - \langle \mathbf{U}^* | \mathbf{X}^* \rangle) dt + \frac{\hat{b}k}{\sqrt{\varepsilon}} d\mathbf{W}' \quad (50)$$

and

$$\frac{d\phi^*}{dt} = -\hat{c}\frac{\varepsilon}{k}(\phi^* - \langle\phi^* | \mathbf{R}^*, \mathbf{X}^*\rangle), \quad (51)$$

with

$$\hat{a} = \frac{a}{C_T}, \quad \hat{b} = b \left(\frac{4}{3}C_T\right)^{1/2}, \quad \hat{c} = \frac{c}{C_T}. \quad (52)$$

For the values  $a = 1$ ,  $b = 1/(1+a) = 1/2$ ,  $c = 3.27$ , and  $C_0 = 2.1$ , corresponding values are  $\hat{a} = 2.1$ ,  $\hat{b} = 0.40$ , and  $\hat{c} = 6.8$ .

## B. Composition PDF method

In Secs. I–V, we have presented and employed the shadow-position mixing model in the context of the velocity-composition PDF approach, in which the particle moves with its own velocity  $\mathbf{U}^*(t)$ , which evolves by a Langevin equation (Eqs. (1) and (2)). The shadow-position mixing model can also be applied in the composition PDF approach, in which the particle velocity is not considered, and instead the position evolves by the SDE<sup>8</sup>

$$d\mathbf{X}^* = (\langle\mathbf{U}\rangle + \nabla\Gamma_T)dt + (2\Gamma_T)^{1/2}d\mathbf{W}, \quad (53)$$

where  $\langle\mathbf{U}(\mathbf{x}, t)\rangle$  is the mean velocity field, and  $\Gamma_T(\mathbf{x}, t)$  is the turbulent diffusivity. For this case, the shadow-position model equations are as before (Eqs. (7) and (8)), but for clarity we denote by  $\bar{a}$ ,  $\bar{b}$ , and  $\bar{c}$  the model coefficients used in the context of the composition PDF approach.

In Appendix C, the shadow-position model with the composition PDF approach is examined for the case of the uniform mean scalar gradient considered in Sec. III. It is found that, in the statistically stationary state, the two different PDF approaches give identical results provided that  $a$  is in the range  $a_{\min} < a \leq 1$ , and that  $\bar{a}$ ,  $\bar{b}$ , and  $\bar{c}$  are given by Eqs. (C6)–(C8). It is argued that matching the variance  $\langle R^{*2} \rangle$  between the two methods is not essential, and, with this condition relaxed, the choice of the two parameters  $\bar{a}$  and  $\bar{b}$  is constrained by a single relation, Eq. (C10). The simplest such model has  $\bar{a} = 4a/(2+a)$ ,  $\bar{b} = 0$ , and  $\bar{c} = c$ , with the only restriction on  $a$  being  $a \geq a_{\min}$ .

## C. Application in large-eddy simulations

Above we have considered the use of the shadow-position mixing model in different PDF methods in the RANS context. Such PDF methods are also used in LES,<sup>4,5,7</sup> and the SPMM is directly applicable. (See Pope<sup>40</sup> for a suitable definition of the PDFs used in the LES context.)

In the LES of a high-Reynolds-number flow, the motions larger than the resolution length scale  $\Delta$  are directly represented, while the effects of the smaller, residual motions are modeled, usually *via* an eddy viscosity,  $\nu_T$ . The appropriate shadow-position model equations for LES remain Eqs. (11) and (10) or (C1), but with different coefficients ( $\bar{a}$ ,  $\bar{b}$ , and  $\bar{c}$ , say), and with the turbulent time scale and diffusivity re-defined as

$$\frac{1}{T_L} = \frac{\nu_T}{\Delta^2} \quad \text{and} \quad \Gamma_T = \sigma^2 T_L = \nu_T. \quad (54)$$

## D. Numerical implementation

For the SPMM to be useful in practice, it is essential to have an accurate and efficient computational implementation. At first sight, the prospects for such an implementation may appear bleak, since it is notoriously difficult to estimate accurately statistics conditioned on multiple quantities such as  $\langle\phi^* | \mathbf{X}^*, \mathbf{R}^*\rangle$ . However, an accurate and efficient method has been developed and will be fully described in a forthcoming paper. The essence of the method is now described.

The method developed is a mesh-free, near-neighbor implementation. On each time step, the  $N$  computational particles are ordered so that adjacent particles in the ordering are near neighbors

in the conditioning ( $\mathbf{X}^*$ ,  $\mathbf{R}^*$ ) space. For the  $n$ th particle, with properties  $\mathbf{X}^{(n)}$ ,  $\mathbf{U}^{(n)}$ ,  $\mathbf{R}^{(n)}$ ,  $\phi^{(n)}$ , the SPMM mixing equation

$$\frac{d\phi^{(n)}}{dt} = -\frac{c}{T_L}(\phi^{(n)} - \langle \phi^* | \mathbf{R}^{(n)}, \mathbf{X}^{(n)} \rangle) \quad (55)$$

is approximated by

$$\frac{d\phi^{(n)}}{dt} = -\frac{c}{T_L}(\phi^{(n)} - \frac{1}{2}[\phi^{(n+1)} + \phi^{(n-1)}]). \quad (56)$$

It may appear that the random quantity  $\frac{1}{2}[\phi^{(n+1)} + \phi^{(n-1)}]$  provides a poor, noisy approximation to the non-random quantity  $\langle \phi^* | \mathbf{R}^{(n)}, \mathbf{X}^{(n)} \rangle$ . The crucial observation is that the statistics given by the SPMM are unaltered if, in Eq. (55),  $\langle \phi^* | \mathbf{R}^{(n)}, \mathbf{X}^{(n)} \rangle$  is replaced by a random composition  $\widehat{\phi}^{(n)}$ , providing that (1) it has the correct conditional mean, i.e.,  $\langle \widehat{\phi}^{(n)} | \mathbf{R}^{(n)}, \mathbf{X}^{(n)} \rangle = \langle \phi^* | \mathbf{R}^{(n)}, \mathbf{X}^{(n)} \rangle$ , and (2) that  $\widehat{\phi}^{(n)}(t)$  is uncorrelated in time. Both of these conditions are satisfied as the number of particles  $N$  tends to infinity, and the time step tends to zero. In these limits, the distance between near neighbors tends to zero (so that (1) is satisfied), and the time taken for the  $n$ th particle to encounter new neighbors also tends to zero (so that (2) is satisfied).

To illustrate the performance of the near-neighbor implementation of SPMM for finite  $N$ , Fig. 19 shows results obtained for the non-premixed-combustion test case considered in Sec. V, with  $\xi_l = 0.03$ ,  $\xi_r = 0.07$ , and  $a = 1.1$ . This value of  $a$  is quite close to the critical value, and so numerical errors can incorrectly lead to extinction. This is indeed observed for  $N = 4000$ , but for the larger number of particles ( $N = 16\,000$ – $256\,000$ ) little dependence on  $N$  is evident. A computation of this case with  $N = 16\,000$  takes 100 s on a 2.7 GHz MacBook Pro using an unoptimized Matlab script.

These results demonstrate that, for the statistically one-dimensional cases considered here, the near-neighbor implementation of SPMM produces accurate calculations at a modest cost. A quantification of the performance of the method and its application to more challenging cases is left to future work. For these cases, it may be that conditioning on one or two components of  $\mathbf{R}^*$  may be sufficient. For example, for two-stream mixing problems, conditioning could be performed based on the component of  $\mathbf{R}^*$  in the direction of the mixture fraction gradient.

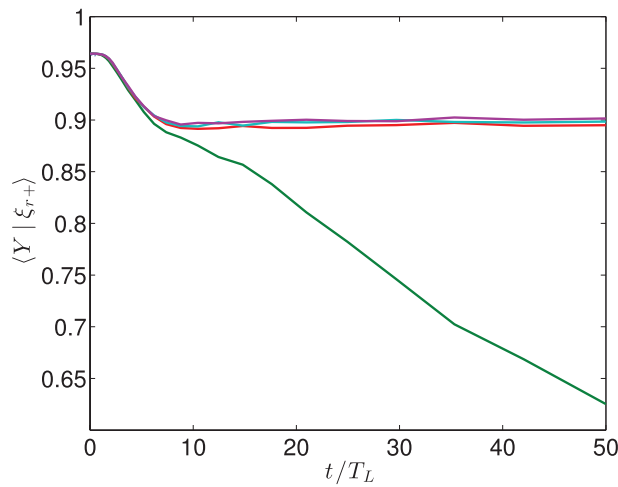


FIG. 19. The temporal evolution of the conditional mean product mass fraction for  $\xi = \xi_{r,+} = 0.084$  according to the SPMM with  $a = 1.1$ , computed using the near-neighbor implementation with  $N$  particles. From bottom to top:  $N = 4000$ , 16 000, 64 000, 256 000.

### E. The velocity-shadow-position mixing model

An obvious extension of SPMM is to consider the *velocity-shadow-position mixing model* (VSPMM) in which conditioning is performed on  $\mathbf{U}^*$ ,  $\mathbf{R}^*$ , and  $\mathbf{X}^*$ . Thus, the SPMM mixing equation (Eq. (11)) is replaced by

$$\frac{d\phi^*}{dt} = -\frac{c_v}{T_L}(\phi^* - \langle \phi^* | \mathbf{U}^*, \mathbf{R}^*, \mathbf{X}^* \rangle), \quad (57)$$

where  $c_v$  is a model coefficient.

An analysis, similar to that performed in Appendix A, shows that the coefficient  $b$  is not constrained by the dispersion-consistency condition. For specified  $b \geq 0$ , there is a minimum value of  $a$ ,  $a_{\min}(b)$ , for which  $c_v$  is infinite, and there are no conditional fluctuations. For  $a > a_{\min}(b)$ , the finite value of  $c_v$  is then determined by the scalar variance.

The principal virtue of VSPMM is that it satisfies the dispersion-consistency condition exactly (for all  $b \geq 0$ ). It is exactly local for  $a = a_{\min}(b)$ , and is approximately so for small  $a - a_{\min}(b)$ . However, the added conditioning variables compound the difficulties of developing an accurate and efficient numerical implementation, and it is unlikely that this model is useful for PDF modeling of inhomogeneous flows.

### F. Determination of shadow-position conditioned statistics in DNS

The shadow position  $\mathbf{Z}^*(t)$  and the shadow displacement  $\mathbf{R}^*(t) \equiv \mathbf{Z}^*(t) - \mathbf{X}^*(t)$  are non-physical quantities, and hence they cannot be measured in an experiment. They can, however, be determined in a DNS, and hence statistics conditional on  $\mathbf{R}^*(t)$  can be extracted. For example, for a single composition with molecular diffusivity  $\Gamma$ , the conditional diffusion from DNS,

$$\mathcal{D}(\psi, \mathbf{x}, \hat{\mathbf{R}}, t) \equiv \langle \Gamma \nabla^2 \phi(\mathbf{x}, t) | \phi = \psi, \mathbf{X}^*(t) = \mathbf{x}, \mathbf{R}^*(t) = \hat{\mathbf{R}} \rangle, \quad (58)$$

can be compared to the form supposed by the shadow-position mixing model

$$\mathcal{D}(\psi, \mathbf{x}, \hat{\mathbf{R}}, t) = -\frac{c}{T_L}(\psi - \langle \phi(\mathbf{x}, t) | \mathbf{X}^*(t) = \mathbf{x}, \mathbf{R}^*(t) = \hat{\mathbf{R}} \rangle). \quad (59)$$

Such conditional statistics can be extracted from DNS by both Lagrangian and Eulerian methods. The straightforward Lagrangian approach is to solve Eq. (10) for a large number of particles to obtain their values of  $\mathbf{R}^*(t)$ .

In the Eulerian approach, the probability distribution of  $\mathbf{R}^*$  is determined by solving Eulerian transport equations for its mean and variance. For a given DNS, we regard the velocity  $\mathbf{U}(\mathbf{x}, t)$  as deterministic, so that the only randomness is due to the Wiener process in the SDE for  $\mathbf{R}^*(t)$ , Eq. (10). This is a linear SDE in the narrow sense, and hence the PDF of  $\mathbf{R}^*$  is Gaussian, determined by its mean and covariance, which evolve by known Eulerian transport equations (see Sec. 8.2 of Arnold<sup>36</sup>). These equations, written in Eulerian form for the mean  $\langle \mathbf{R}(\mathbf{x}, t) \rangle \equiv \langle \mathbf{R}^*(t) | \mathbf{X}^*(t) = \mathbf{x} \rangle$  and the covariance denoted by  $\langle R'_i R'_j \rangle$  are

$$\frac{D\langle \mathbf{R} \rangle}{Dt} = -\frac{a}{T_L} \langle \mathbf{R} \rangle - (\mathbf{U} - \langle \mathbf{U} \rangle) \quad (60)$$

and

$$\frac{D\langle R'_i R'_j \rangle}{Dt} = -\frac{2a}{T_L} \langle R'_i R'_j \rangle + 2b^2 \sigma^2 T_L \delta_{ij}, \quad (61)$$

where  $\langle \mathbf{U}(\mathbf{x}, t) \rangle$  is the mean of  $\mathbf{U}(\mathbf{x}, t)$  over all realizations of the DNS.

For the case of homogeneous turbulence (and any other case in which the length scale  $\sigma T_L$  is uniform), the covariance equation has the constant solution

$$\langle R'_i R'_j \rangle = \frac{(b\sigma T_L)^2}{a} \delta_{ij}, \quad (62)$$

and hence Eq. (61) does not need to be solved numerically.

It is interesting to observe from Eq. (A7) that the normalized variance of  $R^*$  (i.e., a component of  $\mathbf{R}^*$ ) in this case is  $b^2/a + 1/[a(1+a)]^{-1}$ ; and that the first contribution is from  $\langle R^2 \rangle$ , while the second arises from the variance of  $\langle R \rangle$  (over all positions, times, and realizations of the DNS). (The result that the latter contribution equals  $1/[a(1+a)]^{-1}$  depends on the Lagrangian velocity autocorrelation being exponential.)

### G. Statistically homogeneous scalar mixing

In most practical flows involving turbulent mixing, the processes of convective turbulent transport and molecular mixing are inexorably coupled. This is the case for flows in which the fluid enters in streams of different composition, and for flows (such as the atmospheric boundary layer) in which the inhomogeneity of composition arises from heat or mass transfer at a surface, with subsequent turbulent convective transport into the interior. In both the IECM and shadow-position models, the conditioning is based on the velocity responsible for the convective transport; either directly in IECM, or indirectly in SPMM, through the influence of velocity on the shadow displacement (see Eq. (10)).

Many previous studies of turbulent mixing models<sup>3,13,20</sup> have included testing against DNS of statistically homogeneous composition fields evolving from initial conditions, such as randomly located blobs of fluid of different composition, corresponding approximately to delta-function PDFs. Examples include the mixing of a single composition<sup>41</sup> and of two compositions.<sup>42</sup> We now argue that these DNS are not good test cases for mixing models intended for application in the RANS context to inhomogeneous flows, because they artificially separate the processes of convective transport and molecular mixing. As these processes are disconnected, both the IECM model and SPMM in this case reduce to the IEM model, which performs poorly in these tests: delta-function distributions evolve by the locations (in composition space) of the delta functions moving towards the mean, without any relaxation towards a Gaussian.<sup>3</sup>

Instead, here we consider the scalar mixing layer to be the simplest relevant test case because, as in the intended applications, the inhomogeneity in composition arises from different streams of different uniform composition. For this case, the results on skewness and kurtosis presented in Sec. IV show that the SPMM yields distributions similar to those observed experimentally.

The above criticism of the statistically homogeneous DNS test cases applies only to RANS. In LES applied to these flows, convective transport by the resolved scales is appropriately connected to turbulent mixing.

## VII. SUMMARY AND CONCLUSIONS

The shadow-position mixing model—a new model for turbulent mixing—has been presented and its performance demonstrated. To a fluid particle with position  $\mathbf{X}^*(t)$  we associate a shadow particle with position  $\mathbf{Z}^*(t)$ , which is defined to evolve by the SDE Eq. (8). Correspondingly, the shadow displacement  $\mathbf{R}^*(t) \equiv \mathbf{Z}^*(t) - \mathbf{X}^*(t)$  evolves by Eq. (10). Mixing is modeled as a relaxation of the particle composition  $\phi^*(t)$  towards the conditional mean  $\langle \phi^*(t) | \mathbf{Z}^*(t), \mathbf{X}^*(t) \rangle$ , which is the same as  $\langle \phi^*(t) | \mathbf{R}^*(t), \mathbf{X}^*(t) \rangle$ . The significance of conditioning on  $\mathbf{Z}^*$  (or, equivalently, on  $\mathbf{R}^*$ ) is that fluid particles (from different realizations) with the same values of  $\mathbf{X}^*$  and  $\mathbf{Z}^*$  share a similar history.

The shadow-position mixing model is related to previous models—IEM, IECM, and MMC—and indeed, as discussed in Sec. III E, it reduced to these models for limiting values of the model coefficients. The model is constructed to be consistent with turbulent dispersion theory and to be local in composition space, both to an adequate approximation.

The model is applied (in Sec. IV) to a mildly strained scalar mixing layer, and it is shown to yield statistics in broad agreement with the experimental data of Ma and Warhaft<sup>32</sup> (which pertain to a slightly different flow). The model is also applied (in Sec. V) to a reactive scalar mixing layer, and it is shown to yield, correctly, stable burning for a test case of high-Damköhler-number non-premixed combustion, for which the IEM and IECM models, incorrectly, yield extinction.



A simple and reasonable specification of the model coefficient  $a$  is  $a = 1$ , which leads to  $b = 1/2$  and  $c = 3.27$ . This value of  $a$  is small enough to yield, correctly, stable combustion (i.e.,  $a < a_{\text{crit}}$ ), but large enough to allow some level of conditional fluctuations (i.e.,  $a > a_{\text{min}}$ ).

The shadow-position mixing model approaches the localness in composition space achieved by the EMST mixing model,<sup>13</sup> and it avoids the major shortcomings of EMST. Specifically, it avoids “stranding”; it satisfies the linearity and independence principles; it yields Gaussian distributions where appropriate; and it is free of numerical artifacts.

The shadow-position mixing model is developed here primarily for the velocity-composition PDF method in the RANS context for simple flows. In Sec. VI, extensions to general flows, to the composition PDF method, and to LES are described.

Computationally, the shadow-position mixing model has been implemented using a mesh-free, “near-neighbor” algorithm, outlined in Sec. VI D.

An extension of SPMM is the velocity-shadow-position mixing model described in Sec. VI E, which exactly satisfies the dispersion consistency condition, but is less amenable to numerical implementation.

Needless to say, it is desirable in future work to evaluate the performance of the shadow-position mixing model for a broader set of flows than has been considered here. Of particular interest is the mixing of multiple compositions in grid turbulence,<sup>35</sup> in DNS of multiple scalar mixing layers,<sup>43</sup> in co-axial jets,<sup>44</sup> and in DNS of reactive flows.<sup>45</sup> The model holds the promise of representing, more accurately than previous models, turbulent mixing in a broad range of turbulent flows, including turbulent combustion.

## ACKNOWLEDGMENTS

It is a great pleasure to dedicate this paper to Parviz Moin on the occasion of his sixtieth birthday, to honor his many influential contributions to turbulence research. Discussions on this work with Alex Klimenko are gratefully acknowledged. This work is supported by Office of Energy Research, Office of Basic Energy Sciences, Chemical Sciences, Geosciences and Biosciences Division of the U.S. Department of Energy (DOE) under Grant No. DE-FG02-90ER-14128.

## APPENDIX A: SECOND-MOMENT EQUATIONS AND THEIR STATIONARY SOLUTIONS

From Eqs. (22)–(25), we can derive the evolution equations for the first and second moments. Initially, the means  $\langle U^* \rangle$ ,  $\langle R^* \rangle$ , and  $\langle \phi^* \rangle$  are zero, and their evolution equations show that they remain zero.

The evolution equations for the second moments are

$$\frac{d\langle U^{*2} \rangle}{dt} = -\frac{2\langle U^{*2} \rangle}{T_L} + \frac{2\sigma^2}{T_L}, \quad (\text{A1})$$

$$\frac{d\langle U^* R^* \rangle}{dt} = -(1+a)\frac{\langle U^* R^* \rangle}{T_L} - \langle U^{*2} \rangle, \quad (\text{A2})$$

$$\frac{d\langle R^{*2} \rangle}{dt} = -2a\frac{\langle R^{*2} \rangle}{T_L} - 2\langle U^* R^* \rangle + 2b^2\sigma^2 T_L, \quad (\text{A3})$$

$$\frac{d\langle U^* \phi^* \rangle}{dt} = -\frac{\langle U^* \phi^* \rangle}{T_L} - G\langle U^{*2} \rangle - \frac{c}{T_L} \left( \langle U^* \phi^* \rangle - \frac{\langle U^* R^* \rangle \langle R^* \phi^* \rangle}{\langle R^{*2} \rangle} \right), \quad (\text{A4})$$

$$\frac{d\langle R^* \phi^* \rangle}{dt} = -a\frac{\langle R^* \phi^* \rangle}{T_L} - \langle U^* \phi^* \rangle - G\langle U^* R^* \rangle, \quad (\text{A5})$$

$$\frac{d\langle \phi^{*2} \rangle}{dt} = -2G\langle U^* \phi^* \rangle - \frac{2c}{T_L} \left( \langle \phi^{*2} \rangle - \frac{\langle R^* \phi^* \rangle^2}{\langle R^{*2} \rangle} \right). \quad (\text{A6})$$

The statistically stationary solutions to these equations are obtained by setting the left-hand sides to zero. Inevitably and consistently, Eq. (A1) yields  $\langle U^{*2} \rangle = \sigma^2$ . The solutions to Eqs. (A2) and (A3) are

$$\frac{\langle U^* R^* \rangle}{\sigma^2 T_L} = \frac{-1}{(1+a)}, \quad \frac{\langle R^{*2} \rangle}{(\sigma T_L)^2} = \frac{1}{a} \left( b^2 + \frac{1}{1+a} \right). \quad (\text{A7})$$

We require that the model satisfies the dispersion-consistency condition in the statistically stationary state. This means that the term in  $c$  in Eq. (A4) must vanish, and then the equation is indeed consistent with Eq. (20). Substituting the scalar flux given by Eq. (20) into Eq. (A5), we then obtain

$$\frac{\langle R^* \phi^* \rangle}{G \sigma^2 T_L^2} = \frac{2+a}{a(1+a)}. \quad (\text{A8})$$

The condition that the term in  $c$  in Eq. (A4) be zero can be re-expressed as

$$\langle R^{*2} \rangle \langle U^* \phi^* \rangle = \langle U^* R^* \rangle \langle R^* \phi^* \rangle, \quad (\text{A9})$$

and substituting the relations obtained above for the second moments, we obtain the following condition that the coefficients must satisfy in order for the model satisfy the dispersion-consistency condition in the statistically stationary state:

$$b = \frac{1}{1+a}. \quad (\text{A10})$$

With this specification of  $b$ , we then obtain from Eq. (A7)

$$\frac{\langle R^{*2} \rangle}{(\sigma T_L)^2} = \frac{2+a}{a(1+a)^2}. \quad (\text{A11})$$

Substituting the above results into Eq. (A6), we obtain that the stationary scalar variance is

$$V_\phi \equiv \frac{\langle \phi^{*2} \rangle}{(G \sigma T_L)^2} = \frac{1}{c} + \frac{2+a}{a}. \quad (\text{A12})$$

The correlation coefficients are readily obtained from Eqs. (20), (A7), (A8), (A11), and (A12), and are given in the text as Eqs. (30)–(32).

## APPENDIX B: THE MEAN PROFILE IN THE SCALAR MIXING LAYER

In this appendix, turbulent dispersion theory is used to show that, for the scalar mixing layer considered in Sec. IV, the mean scalar  $\langle \phi(x, t) \rangle$  has the error-function profile

$$\begin{aligned} \langle \phi(x, t) \rangle &= \int_{-\infty}^x \frac{1}{\sigma_X \sqrt{2\pi}} \exp\left(-\frac{z^2}{2\sigma_X^2}\right) dz \\ &= \frac{1}{2} \left[ 1 + \operatorname{erf}\left(\frac{x}{\sigma_X \sqrt{2}}\right) \right], \end{aligned} \quad (\text{B1})$$

where  $\sigma_X(t)$  is given by Eq. (B10).

The particle position evolves by Eq. (43), in which  $S$  is the specified constant mean strain rate, and  $U^*(t)$  is the solution to the Langevin equation, i.e., an Ornstein-Uhlenbeck (OU) process, with mean zero, variance  $\sigma^2$ , and time scale  $T_L$ . The straining has the effect of concentrating the particles in  $x$ , and to account for this effect, it is necessary to include a particle weight  $m^*(t)$  which evolves by

$$\frac{dm^*}{dt} = -S m^*, \quad (\text{B2})$$

from the initial condition  $m^*(0) = 1$ , which has the deterministic solution

$$m^*(t) = \exp(-St). \quad (\text{B3})$$

We denote by  $f(x; y, t)$  the PDF of  $X^*(t)$  conditional on  $X^*(0) = y$ . Then the standard application of turbulent dispersion theory yields for the mean profile

$$\langle \phi(x, t) \rangle = \int_{-\infty}^{\infty} H(y) f(x; y, t) m(t) dy, \quad (\text{B4})$$

where the integration is over the source distribution  $H(y)$  at time  $t = 0$ . Or, equivalently, the integral gives the probability that the particle at  $x$  at time  $t$  originated from  $x \geq 0$  at  $t = 0$ , and therefore (in the absence of molecular diffusion) has the scalar value  $\phi^*(t) = \phi^*(0) = 1$ .

It is evident from Eq. (43) that the PDF  $f(x; y, t)$  is Gaussian, with mean

$$\langle X^*(t) | X^*(0) = y \rangle = y \exp(-St), \quad (\text{B5})$$

and we denote by  $\sigma_X^2$  the variance of  $(X^*(t) | X^*(0) = y)$ , which is the same as the variance of  $[X^*(t) - X^*(0)]$ , and is independent of  $y$ . The result that  $\langle \phi(x, t) \rangle$  has the error-function profile given by Eq. (B1) is obtained by substituting into Eq. (B4) the known Gaussian for  $f(x; y, t)$  with mean  $y \exp(-St)$  and variance  $\sigma_X^2$ , with the substitution  $z \equiv \exp(-St) - x$ .

It remains to determine the width of the scalar mixing layer  $\sigma_X(t)$ , which is the standard deviation of  $[X^*(t) - X^*(0)]$ . The particle position equation, Eq. (43), can be integrated to yield

$$X^*(t) - X^*(0) = \int_0^t \exp(-S[t-t']) U^*(t') dt', \quad (\text{B6})$$

and hence we obtain

$$\sigma_X^2 = \langle [X^*(t) - X^*(0)]^2 \rangle = \int_0^t \int_0^t \exp(-S[t-t']) \exp(-S[t-t'']) \langle U^*(t') U^*(t'') \rangle dt' dt''. \quad (\text{B7})$$

Substituting the known autocovariance

$$\langle U^*(t') U^*(t'') \rangle = \sigma^2 \exp\left(-\frac{|t' - t''|}{T_L}\right), \quad (\text{B8})$$

and performing the integrations, we obtain the required result: for the case  $ST_L = 1$  it is

$$\sigma_X^2 = \frac{1}{2} \left(\frac{\sigma}{S}\right)^2 [1 - (1 + 2St) \exp(-2St)]; \quad (\text{B9})$$

and, for the case  $ST_L \neq 1$ , with the definition  $\eta \equiv 1/(ST_L)$ , it is

$$\sigma_X^2 = \left(\frac{\sigma}{S}\right)^2 \left( \frac{2 \exp(-St[1 + \eta]) - (1 + \eta) \exp(-2St) + \eta - 1}{(\eta^2 - 1)} \right). \quad (\text{B10})$$

In the statistically stationary state, the width of the layer is

$$\sigma_X(\infty) = \left(\frac{\sigma}{S}\right) \frac{1}{\sqrt{1 + \eta}}. \quad (\text{B11})$$

## APPENDIX C: COMPOSITION PDF APPROACH

In the context of the composition PDF approach, the evolution equations for  $\mathbf{X}^*(t)$ ,  $\mathbf{Z}^*(t)$ , and  $\phi^*(t)$  are Eqs. (53), (8), and (11) (with  $a$ ,  $b$ , and  $c$  replaced by  $\bar{a}$ ,  $\bar{b}$ , and  $\bar{c}$ ). We consider here the application of this model to the case of the uniform mean scalar gradient considered in Sec. III.

For the case considered, the turbulent viscosity is given by  $\Gamma_T = \sigma^2 T_L$  (Eq. (19)). Because the particle position evolves by the SDE Eq. (53), in place of Eqs. (23) and (24), the evolution equations for  $R^*(t)$  and  $\phi^*(t)$  are the SDEs

$$dR^* = -\bar{a} R^* \frac{dt}{T_L} + (2\Gamma_T)^{1/2} (\bar{b} dW' - dW) \quad (\text{C1})$$

and

$$d\phi^* = -\bar{c}(\phi^* - \langle \phi^* | R^* \rangle) \frac{dt}{T_L} - G(2\Gamma_T)^{1/2} dW. \quad (\text{C2})$$

An analysis of the second-moment equations for  $\langle R^{*2} \rangle$ ,  $\langle R^* \phi^* \rangle$ , and  $\langle \phi^{*2} \rangle$ , similar to that performed in Appendix A, shows that their values in the statistically stationary state are

$$\frac{\langle R^{*2} \rangle}{(\sigma T_L)^2} = \frac{1 + \bar{b}^2}{\bar{a}}, \quad (\text{C3})$$

$$\frac{\langle R^* \phi^* \rangle}{(\sigma T_L)^2 G} = \frac{2}{\bar{a}}, \quad (\text{C4})$$

$$\frac{\langle \phi^{*2} \rangle}{(\sigma T_L G)^2} = \frac{1}{\bar{c}} + \frac{4}{\bar{a}(1 + \bar{b}^2)}. \quad (\text{C5})$$

It is readily deduced that these moments for the composition PDF method are identical to those given by the velocity-composition PDF method (Eqs. (A11), (A8), and (A12)), provided that the coefficients  $\bar{a}$ ,  $\bar{b}$ , and  $\bar{c}$  are related to  $a$  and  $c$  by

$$\bar{a} = a \left( \frac{1 + a}{1 + \frac{1}{2}a} \right), \quad (\text{C6})$$

$$\bar{b} = \left( \frac{1 - a}{1 + a} \right)^{1/2}, \quad (\text{C7})$$

$$\bar{c} = c = \frac{1}{2} \left( \frac{1}{a_{\min}} - \frac{1}{a} \right)^{-1}. \quad (\text{C8})$$

It is evident from Eqs. (C7) and (C8) that these equations can be satisfied (for real, positive  $\bar{a}$  and  $\bar{c}$ ) only for  $a$  in the quite narrow range  $a_{\min} < a \leq 1$ .

It can be argued, however, that matching the variance  $\langle R^{*2} \rangle$  may not be crucial or even necessary. The shadow displacement  $R^*$  enters the model solely through the conditional mean  $\langle \phi^* | R^* \rangle$ , and in the Gaussian approximation this is

$$\langle \phi^* | R^* \rangle = \frac{R^*}{\langle R^{*2} \rangle^{1/2}} \langle \phi^{*2} \rangle^{1/2} \rho_{R\phi}. \quad (\text{C9})$$

Thus,  $R^*$  enters the model only in its standardized form  $R^*/\langle R^{*2} \rangle^{1/2}$ , and hence (at least to the Gaussian approximation) the model is unaffected by the magnitude of the variance  $\langle R^{*2} \rangle$ . It follows from the second-moment equations that matching  $\langle \phi^{*2} \rangle$  and  $\rho_{R\phi}$  is achieved provided that the coefficients satisfy  $\bar{c} = c$  and

$$\bar{a}(1 + \bar{b}^2) = \frac{4a}{2 + a}. \quad (\text{C10})$$

The simplest model consistent with this requirement is  $\bar{b} = 0$ ,  $\bar{a} = 4a/(2 + a)$ .

- <sup>1</sup>Z. Warhaft, "Passive scalars in turbulent flows," *Annu. Rev. Fluid Mech.* **32**, 203–240 (2000).
- <sup>2</sup>S. B. Pope, "PDF methods for turbulent reactive flows," *Prog. Energy Combust. Sci.* **11**, 119–192 (1985).
- <sup>3</sup>R. O. Fox, *Computational Models for Turbulent Reactive Flows* (Cambridge University Press, New York, 2003).
- <sup>4</sup>D. C. Haworth, "Progress in probability density function methods for turbulent reacting flows," *Prog. Energy Combust. Sci.* **36**, 168–259 (2010).
- <sup>5</sup>P. Givi, "Filtered density function for subgrid scale modeling of turbulent combustion," *AIAA J.* **44**, 16–23 (2006).
- <sup>6</sup>D. C. Haworth and S. B. Pope, "Transported probability density function methods for Reynolds-averaged and large-eddy simulations," in *Turbulent Combustion*, edited by T. Echehki and E. Mastorakos (Springer, 2011), pp. 119–142.
- <sup>7</sup>S. B. Pope, "Small scales, many species and the manifold challenges of turbulent combustion," *Proc. Combust. Inst.* **34**, 1–31 (2013).
- <sup>8</sup>S. B. Pope, *Turbulent Flows* (Cambridge University Press, Cambridge, 2000).
- <sup>9</sup>S. B. Pope, "Simple models of turbulent flows," *Phys. Fluids* **23**, 011301 (2011).
- <sup>10</sup>J. Villermaux and J. C. Devillon, "Représentation de la coalescence et de la redispersion des domaines de ségrégation dans un fluide par un modèle d'interaction phénoménologique," in *Proceedings of the 2nd International Symposium on Chemical Reaction Engineering* (Elsevier, New York, 1972), pp. 1–13.
- <sup>11</sup>C. Dopazo and E. E. O'Brien, "An approach to the autoignition of a turbulent mixture," *Acta Astronaut.* **1**, 1239–1266 (1974).
- <sup>12</sup>S. B. Pope, "An improved turbulent mixing model," *Combust. Sci. Technol.* **28**, 131–145 (1982).

- <sup>13</sup> S. Subramaniam and S. B. Pope, "A mixing model for turbulent reactive flows based on Euclidean minimum spanning trees," *Combust. Flame* **115**, 487–514 (1998).
- <sup>14</sup> G. I. Taylor, "Diffusion by continuous movements," *Proc. London Math. Soc.* **s2-20**, 196–212 (1922).
- <sup>15</sup> S. B. Pope, "The vanishing effect of molecular diffusivity on turbulent dispersion: implications for turbulent mixing and the scalar flux," *J. Fluid Mech.* **359**, 299–312 (1998).
- <sup>16</sup> S. B. Pope, "On the relationship between stochastic Lagrangian models of turbulence and second-moment closures," *Phys. Fluids* **6**, 973–985 (1994).
- <sup>17</sup> R. O. Fox, "On velocity-conditioned scalar mixing in homogeneous turbulence," *Phys. Fluids* **8**, 2678–2691 (1996).
- <sup>18</sup> B. L. Sawford, "Micro-mixing modelling of scalar fluctuations in plumes in homogeneous turbulence," *Flow, Turbul. Combust.* **72**, 133–160 (2004).
- <sup>19</sup> S. Viswanathan and S. B. Pope, "Turbulent dispersion behind line sources in grid turbulence," *Phys. Fluids* **20**, 101514 (2008).
- <sup>20</sup> A. T. Norris and S. B. Pope, "Turbulent mixing model based on ordered pairing," *Combust. Flame* **83**, 27–42 (1991).
- <sup>21</sup> R. R. Cao, H. Wang, and S. B. Pope, "The effect of mixing models in PDF calculations of piloted jet flames," *Proc. Combust. Inst.* **31**, 1543–1550 (2007).
- <sup>22</sup> S. B. Pope, "Consistent modeling of scalars in turbulent flows," *Phys. Fluids* **26**, 404–408 (1983).
- <sup>23</sup> A. Y. Klimenko and S. B. Pope, "A model for turbulent reactive flows based on multiple mapping conditioning," *Phys. Fluids* **15**, 1907–1925 (2003).
- <sup>24</sup> A. Y. Klimenko, "Matching conditional moments in PDF modelling of nonpremixed combustion," *Combust. Flame* **143**, 369–385 (2005).
- <sup>25</sup> M. J. Cleary and A. Y. Klimenko, "A detailed quantitative analysis of sparse-Lagrangian filtered density function simulations in constant and variable density reacting jet flows," *Phys. Fluids* **23**, 115102 (2011).
- <sup>26</sup> R. L. Curl, "Dispersed phase mixing: I. Theory and effects of simple reactors," *AIChE J.* **9**, 175–181 (1963).
- <sup>27</sup> J. Janicka, W. Kolbe, and W. Kollmann, "Closure of the transport equation for the probability density function of turbulent scalar fields," *J. Non-Equilib. Thermodyn.* **4**, 47–66 (1977).
- <sup>28</sup> L. Valiño and C. Dopazo, "A binomial Langevin model for turbulent mixing," *Phys. Fluids A* **3**, 3034–3037 (1991).
- <sup>29</sup> D. W. Meyer and P. Jenny, "A mixing model for turbulent flows based on parameterized scalar profiles," *Phys. Fluids* **18**, 035105 (2006).
- <sup>30</sup> D. W. Meyer and P. Jenny, "A mixing model providing joint statistics of scalar and scalar dissipation rate," *Proc. Combust. Inst.* **32**, 1613–1620 (2009).
- <sup>31</sup> M. Hegetschweiler, B. T. Zoller, and P. Jenny, "Reactive parametrized scalar profiles (R-PSP) mixing model for partially premixed combustion," *Combust. Flame* **159**, 734–747 (2012).
- <sup>32</sup> B.-K. Ma and Z. Warhaft, "Some aspects of the thermal mixing layer in grid turbulence," *Phys. Fluids* **29**, 3114–3120 (1986).
- <sup>33</sup> M. R. Overholt and S. B. Pope, "Direct numerical simulation of a passive scalar with imposed mean gradient in isotropic turbulence," *Phys. Fluids* **8**, 3128–3148 (1996).
- <sup>34</sup> P. K. Yeung, S. Xu, and K. R. Sreenivasan, "Schmidt number effects on turbulent transport with uniform mean scalar gradient," *Phys. Fluids* **14**, 4178–4191 (2002).
- <sup>35</sup> Z. Warhaft, "The interference of thermal fields from line sources in grid turbulence," *J. Fluid Mech.* **144**, 363–387 (1984).
- <sup>36</sup> L. Arnold, *Stochastic Differential Equations: Theory and Applications* (John Wiley, New York, 1974).
- <sup>37</sup> S. M. de Bruyn Kops and M. Mortensen, "Conditional mixing statistics in a self-similar scalar mixing layer," *Phys. Fluids* **17**, 095107 (2005).
- <sup>38</sup> S. P. Burke and T. E. W. Schumann, "Diffusion flames," *Ind. Eng. Chem.* **20**, 998–1005 (1928).
- <sup>39</sup> F. A. Williams, *Combustion Theory* (Benjamin Cummings, Menlo Park, 1985).
- <sup>40</sup> S. B. Pope, "Self-conditioned fields for large-eddy simulations of turbulent flows," *J. Fluid Mech.* **652**, 139–169 (2010).
- <sup>41</sup> V. Eswaran and S. B. Pope, "Direct numerical simulations of the turbulent mixing of a passive scalar," *Phys. Fluids* **31**, 506–520 (1988).
- <sup>42</sup> A. Juneja and S. B. Pope, "A DNS study of turbulent mixing of two passive scalars," *Phys. Fluids* **8**, 2161–2184 (1996).
- <sup>43</sup> B. L. Sawford and S. M. de Bruyn Kops, "Direct numerical simulation and Lagrangian modeling of joint scalar statistics in ternary mixing," *Phys. Fluids* **20**, 095106 (2008).
- <sup>44</sup> J. Cai, M. J. Dinger, W. Li, C. D. Carter, M. D. Ryan, and C. Tong, "Experimental study of three-scalar mixing in a turbulent coaxial jet," *J. Fluid Mech.* **685**, 495–531 (2011).
- <sup>45</sup> E. R. Hawkes, R. Sankaran, J. C. Sutherland, and J. H. Chen, "Scalar mixing in direct numerical simulations of temporally evolving plane jet flames with skeletal CO/H<sub>2</sub> kinetics," *Proc. Combust. Inst.* **31**, 1633–1640 (2007).